SINGLE CELL MICROINJECTION USING COMPLIANT FLUIDIC CHANNELS AND ELECTROOSMOTIC DOSAGE CONTROL

SINGLE CELL MICROINJECTION USING COMPLIANT FLUIDIC CHANNELS AND ELECTROOSMOTIC DOSAGE CONTROL

BY

ARASH NOORI

B.ENG.MGMT. (MECHANICAL ENGINEERING & MANAGEMENT)

A Thesis

Submitted to the School of Graduate Studies

in Partial Fulfillment of the Requirements for the Degree of Master of Applied Science

McMaster University

MASTER THESIS (2008)	MCMASTER UNIVERSITY
(Mechanical Engineering)	Hamilton, Ontario, Canada
TITLE:	SINGLE CELL MICROINJECTION USING COMPLIANT FLUIDIC CHANNELS AND ELECTROOSMOTIC DOSAGE CONTROL
AUTHOR:	Arash Noori, B.Eng.Mgmt.
SUPERVISOR:	Dr. P.R. Selvaganapathy
NUMBER OF PAGES:	xiii, 86

ABSTRACT

The introduction of bio-molecules into cells and embryos is required in the fields of drug development, genetic engineering and in-vitro fertilization. It has been applied to create transgenic mammals and to improve pest and mold resistance in plants. However, the efficient transfection of materials still poses a problem, and a variety of techniques, broadly classified as biochemical and physical means, are actively being developed. One technique that is promising is capillary microinjection as it offers low cytotoxicity, targeted injections and high transfection efficiency. However, this process suffers from low throughput and variability as it is an operator mediated process. Other problems associated with capillary microinjection are limitations on the minimum needle size and variability in transfected volumes due to the use of pressure driven flow for injections. In this thesis we propose a device that employs microfluidic principles to enable cell microinjections in a 'lab on a chip' format and eliminates the problems associated with capillary microinjection.

The device is fabricated using poly dimethylsiloxane (PDMS) rapid prototyping and features two separate channel structures – one to supply the targets and the other to supply the reagent. Integrated into the device are a microinjection capillary (10 μm tip diameter) and a suction capillary (0.5mm ID/1mm OD) which is used to immobilize the targets in the channel prior to injection. The actuation of the injection needle into the targets is achieved by the compliant deformation of the flexible PDMS substrate as a result of an externally applied displacement. This is made possible by the selective reinforcement of the PDMS substrate. From testing it was found that the effective needle actuation is 83.8% of the externally applied displacement. The injections occur in a planar configuration therefore providing precise control over the location of injection. Furthermore, the mechanism requires only one degree of freedom to perform injections, and therefore greatly simplifies existing injection techniques which require orientation in a three dimensional space.

The limitations of the use of pressure driven flow for injections are overcome by performing reagent injection by electroosmotic flow, which is induced by applying a potential to electrodes embedded in the target and reagent supply channels. The applied potential induces electroosmotic flow through the embedded needle and into the injection target. This provides precise electrical dosage control. The flow rates were obtained by measuring the velocity of the interface between a neutral fluorescent marker and a clear pH 10 buffer solution. The obtained flow rates follow a predictable linear trend and correspond well to theory. The use of electroosmotic flow enables the use of smaller injection needles as it scales more favorably (r^{-2}) than pressure driven flow (r^{-4}) and becomes increasingly dominant in smaller dimensions. Present pressure microinjection systems are limited to injection needles with tip diameters larger than 0.2μm due to the high pressures required to dose at smaller dimensions.

All components of the device are fully scalable and enable further miniaturization, multiple parallel injections and autonomous functionality. The device requires smaller volumes of samples and expensive reagents and also reduces the time required for performing injections. Overall, it device maintains the advantages of microinjection, while eliminating problems of low throughput, dosage control and restrictions on the injection needle size. The device was successfully used and characterized for the injection of single-cell Xenopus Laevis eggs and Zebrafish embryos.

ACKNOWLEDGEMENTS

First and foremost I would like to thank my advisor Professor Selvaganapathy for giving me the opportunity to work with him in this fascinating field of research. Entering the realm of microfluidics from a traditional mechanical engineering background was a great challenge; however his patience, encouragement and wealth of knowledge made this seemingly formidable challenge surmountable. He always encouraged creativity, "out the box" thinking and independence, but provided guidance whenever it was required. The knowledge and lessons learned, however, were not just topical. Not only did I gain a solid background in microfluidics and microfabrication, but more importantly, I learned to approach problems without apprehension or fear, and that with patience and ingenuity any problem could be resolved. This has instilled in me a deep sense of confidence which will always remain with me.

Another source of support and inspiration were my lab mates Bala, Pouya, Geetha, Wen, Mohamed and Simon who offered their help whenever they could. Working with these great people made my time in the lab truly enjoyable. I would also like to thank Professor Ching for the guidance and support he provided me with over the course of my Masters and going as far back as my undergraduate years. He was always available to answer questions regarding my research and the overall course of my academic career. Additionally, I would like to thank Professor Sklad for his help and support which enabled me to pursue my academic goals. Lastly, I owe many thanks to Doris, Zhilin and Graham from the CEDT and Mark Mackenzie for providing equipment and safety training which enabled me to conduct my research.

The encouragement and support, the inspiration and knowledge gained will remain with me always. For this I am forever grateful. Without the guidance and support of the many great people I had the pleasure of working with I would not be where I am today.

TABLE OF CONTENTS

LIST OF FIGURES

LIST OF TABLES

LIST OF EQUATIONS

CHAPTER 1
MOTIVATION AND ORGANIZATION

1.1 Motivation

The introduction of material into cells and embryos is widely used for drug development, genetic engineering and in-vitro fertilization. A variety of techniques which can be broadly classified as biochemical and physical are presently used for this purpose. However, the efficient transfection of materials still poses a problem. One method that is widely used is capillary pressure microinjection. This technique has a number of advantages over other methods, such as high transfection efficiency and low cytotoxicity, however it suffers from low throughput and variability due to operator mediated injections and because of the use of pressure driven flow for reagent transport. In this thesis we present a device that addresses these problems by allowing the injections to be performed in a 'lab on a chip' format with precise electroosmotic dosage control and high throughput. The development of this device will potentially enable the use of capillary microinjection for large scale clinical usage, which can greatly benefit from the advantages that microinjection has to offer over other methods.

1.2 Organization

The organization of the chapters in this thesis is as follows:

Chapter 2 provides an introduction to microfluidics and cell injection techniques. It provides a contrast and comparison of the methods that are currently used for the insertion of bio-molecules into cells and provides an overview of the application of microfluidics in cell transfection.

Chapter 3 introduces our proposed design and explains the advantages of our device over existing techniques. It details the functionality and usage of the device, and highlights its potential for high-throughput. It discusses the design parameters and concludes with an overview of the progression of the design.

Chapter 4 introduces the fabrication techniques and materials used in the assembly of the device. It provides an overview of the device assembly process, the setup and operation of the device.

Chapter 5 describes the experimental setup and the characterization of the device and presents the results obtained from the device. It details the characterization of the compliant actuation mechanism as well as the electroosmotic flow used to perform the injections. It contains simulations performed on the actuation mechanism and electrical measurements obtained from the flow characterization. The chapter concludes with the results, specifically, the injection of Xenopus Laevis eggs with food coloring and the injection of Zebrafish embryos with a methylene blue and Rhodamine buffer solution.

Chapter 6 concludes this thesis by highlighting the contributions of the research, namely, performing injections in a 'lab on a chip' format, the use of compliant fluidic channels and electroosmotic dosage control. It then provides a number of suggestions for the future development of the device.

CHAPTER 2
LITERATURE REVIEW

2.1 Introduction

The introduction of bio-molecules into cells and embryos is required in the fields of drug development, genetic engineering and in-vitro fertilization. It has been applied to create transgenic mammals [Wall 1997], improve pest and mold resistance in plants [Jahne 1995], and most notably, to reprogram human skin cells into induced pluripotent stem cells (iPS), which are similar to embryonic stem (ES) cells, and could potentially be used to create patient-specific stem cells [Takahashi 2007]. However, the efficient transfection of materials still poses a problem [Mehier-Humbert 2004]. This chapter provides an introduction to the methods that are currently used for the insertion of bio-molecules into cells and provides an overview of the application of microfluidics for cell transfection.

2.2 Introduction to Microfluidics

The field of microfluidics involves the precise control and manipulation of small volumes of liquids inside microchannels with sub-millimeter dimensions. Microfluidic devices enable the miniaturizing and integration of multiple laboratory devices and operations into a miniaturized device. Interest in microfluidic 'lab on a chip' devices has increased greatly in recent years. The primary advantage is that these devices require

smaller volumes of samples and expensive reagents and also reduce the time required for performing of analysis since operations can be performed in parallel and with greater speed and accuracy when working with smaller volumes [Sedgwick 2008]. Another advantage is that the fabrication techniques used allow for the fabrication of many devices in parallel, thus leading to reduced manufacturing time and cost [Noori 2008]. Additionally, they enable portability and real-time analysis. A great variety of microfluidic devices have been developed, including portable diagnostic devices for the detection of diseases such as diabetes [Pugia 2005], HIV [Sia 2004], and cancer [Pilarski 2004]. They are also being developed for drug discovery applications [Dittrich 2006], polymerase chain reaction [Zhang 2005], and DNA sequencing [Paegel 2003]. Other examples include microprocessor cooling [Paik 2008], ink jet printing [Bassous 1977], micro chemical reactors [Jensen 2001] and micro fuel cells [Nguyen 2006].

2.3 Physics of Microfluidics

A number of unique phenomena can be exploited in microchannels due to the effects of scaling. The scaling of the surface to volume ratio results in surface effects such as surface tension becoming significantly more important than volume effects such as inertial and gravitational forces [Squires 2005]. Viscous forces dominate over inertial forces, therefore flows in the micro scale are generally laminar ($Re<<1$) and mixing occurs mostly only due to molecular diffusion [Beebe 2002]. Scaling also results in the exponential (L^{-4}) growth in the amount of pressure required to drive fluids in microchannels, making pressure driven flow impractical. However, it also enables electrokinetic effects such as electroosmosis and electrophoresis, which also scale more favorably (L^{-2}) and become dominant in the micro scale [Squires 2005]. Overall, the unique physics in the micro scale have enabled a number of unique applications which would not be possible in the macro scale.

2.4 Introduction to Cell Transfection

Cell transfection techniques can be broadly classified as biochemical and physical methods. Physical methods such as electroporation, sonoporation and capillary microinjection best lend themselves to miniaturization and thus will be the primary focus of this literature review.

2.5 Biochemical Methods

Biochemical methods consist of biological and chemical methods used to transfect materials into cells. Biological techniques make use of viral vectors to introduce DNA into cells. This method is highly efficient, as many viruses have evolved complex mechanisms to overcome cellular barriers. However, viral vector methods suffer from high cytotoxicity, restricted targeting of specific cell types, limited carrying capacity, production problems and high costs [Luo 1999]. Furthermore, there are concerns associated with the use of viral vectors for applications in humans, such as neutralization by serum anti-bodies and immunogenic reactions [Parker 2003].

The concerns associated with the use of viral vectors in humans, has led to the development of synthetic chemical vectors such as lipoplexes (liposome complexes) to allow delivery of material into cells. Prior to delivery, negatively charged DNA molecules are complexed with uptake enhancing cationic transfection reagents [Luo 1999]. These complexes then bind to cells and are internalized, typically by endocytosis. Although this approach is relatively simple and safe, efficiency remain extremely poor due to low uptake across the plasma membrane, inadequate release of DNA molecules and lack of nuclear targeting [Luo 1999].

2.6 Physical Methods

A major barrier to efficiency in intracellular injection is the degradation caused by enzymes within the cells' cytoplasm. Physical methods such as the gene gun, electroporation, sonoporation and capillary microinjection overcome some of these barriers by forming openings in the cell membrane to introduce DNA into the cytoplasm therefore avoiding endosomal and possibly lysomal degradation [Mehier-Humbert 2004]. The aforementioned methods achieve this through particle bombardment, the application of electric fields or ultrasound to cause transient changes in the membrane permeability, or by the insertion of a microinjection capillary, respectively. These methods are discussed in more detail in the following sections.

2.6.1 Gene Gun

The principle of particle bombardment is used in the gene gun transfection technique. In this method naked DNA plasmids are precipitated onto particles that act as carriers to transfer the material into the target cells. This method was developed and first used in 1987 for the insertion of genetic material into plant cells, and was extended to mammalian cells in the 1990s [Parker 2003]. The particles used to carry the plasmid material must be non-toxic, inert, and smaller than the cells to be transfected [Mehier-Humbert 2004]. Initial experiments employed a gunpowder acceleration system to propel DNA-coated tungsten particles into cells [Parker 2003]. The naked DNA that is precipitated on these particles is gradually released after it enters the cell, and thus results in gene expression. A number of factors affect the efficiency of this delivery technique, including the particle size, the distribution and number of DNA-coated particles and concentration of DNA plasmid that is coated onto the particles [Matthews 1993]. A major limitation to gene transfection using particle bombardment is the limited DNA carrying capacity of carrier particles, which also limits successful transfection. Transfection rates can be increased by increasing the number of carrier particles

introduced into the cells – however, increased transfection efficiency is directly related to increased cytotoxicity [Mehier-Humbert 2004].

2.6.2 Electroporation

Electroporation involves the formation of transient and reversible holes or pores in the cell membrane by the application of high intensity electric pulses [Gehl 2003]. This technique requires a pulse generator and an applicator which includes the electrodes. The pores that are created as a result of the applied potential are large enough to allow exogenous micro and macromolecules in the surrounding medium to enter or leave the cell [Potter 1988]. This technique takes advantage of the fact that the cell membrane behaves like capacitor and is unable to conduct current, except through the ion channels. The application of a sufficiently large potential across the membrane will cause a localized destabalization of this barrier. The potential induced across the cell membrane by an applied external electric field is described by [Gehl 2003]:

$$\Delta V_m = f\, E_{ext}\, r \cos\Phi$$

Equation 1: Potential induced across cell membrane by electric field

where V_m is the potential across the cell membrane, f is a factor describing the impact of the cell on the electric field distribution; E_{ext} is the applied electric field, r the cell radius and Φ the polar angle measured from the center of the cell relative to the direction of the external field. The factor f is typically listed as 1.5, however it can vary as it is dependent on a number of different factors [Gehl 2003]. The configuration for a conventional electroporation system with a uniform electric field is shown in Figure 1.

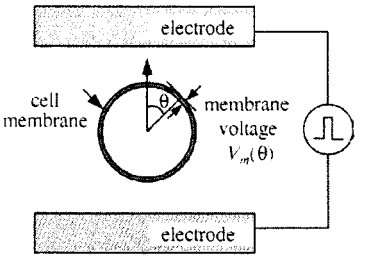

Figure 1: Electroporation in a uniform electric field [Kurosawa 2006]

To ensure that the cell membrane is permeablized it is necessary that the applied electric field surpasses a critical threshold value. The required trans-membrane potential is generally reported to be in the order of 1 V, and is similar for the various eukaryotic cell types due to structural similarities [Gehl 2003]. The degree of permeabilization can be controlled by the pulse duration. The longer the pulse (typically in the range of microseconds), the greater the permeabilization of the membrane. Additionally, as the size of the cell becomes smaller, the external field needed to achieve permeabilization of its membrane increases. Therefore, electric fields used for mammalian cells are considerably lower than those required to permeabilize bacteria, and small intracellular organelles such as the mitochondria are not permeabilized by electric fields used to permeabilize the cell membrane [Potter 1988]. The size of the pores generated as a result of the permeabilization varies between cell types, but was shown to be between 20-120nm in red blood cells, with resealing happening over a range of seconds [Mehier-Humbert 2004]. The precise mechanism by which these pores are formed and closed remains subject to further study and the mechanism by which molecules are transported into the pores also remains unresolved [Mehier-Humbert 2004]. It has been suggested that only molecules bound to the membrane can be internalized by cells or that diffusion and electrophoresis may play a role in transporting molecules in the close proximity of the cell membrane [Gehl 2003].

A number of microfluidic and miniaturized electroporation systems have been developed for the transfection of reagents into endothelial cells [Lin 2003], HeLa cells [Ionescu-Zanetti 2008, Khine 2007], Chinese Hamster Ovarian cells [Wang 2006], human monocytes [Kurosawa 2006], human prostate cells [Huang 2003] and mouse myoblastic cells [Velero 2007]. Existing devices employ a variety of different electrode geometries, as shown in Figure 2.

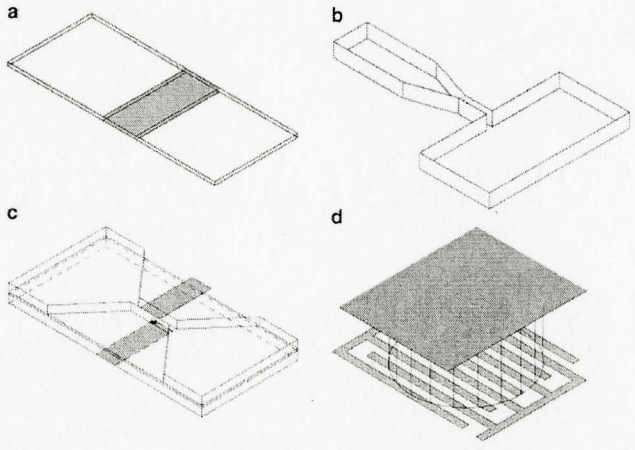

Figure 2: (adapted from Fox 2006) Electrode geometries [Lin 2001, Khine 2006, Huang 2003, Lin 2003]

The advantage of electroporation is that it allows for virtually any type of molecule to be transfected into any type of cell. The process features efficiency typically around 30% [Mehier-Humbert 2004]. The efficiency of the trans-membrane transfection is governed by various physical and biological factors such as the pulse length, electric field strength, the size of the cell and the concentration of the reagent in the medium [Gehl 2003]. As a result of this, the optimal parameters required for electroporation vary across cell types and are also dependent on the size of the molecules to be internalized. A major disadvantage is that it provides only limited and non-quantitative reagent transfection, and degradation by enzymes within the cytoplasm remains a problem as electroporation

lacks the nuclear targeting capability and relies on the diffusion of the internalized molecules into the cell nucleus [Gehl 2003]. Additionally, increased transfection efficiency in electroporation is directly related to increased cytotoxicity [Mehier-Humbert 2004].

2.6.3 Sonoporation

Sonoporation is similar to electroporation in that it introduces exogenous molecules into the cytoplasm by forming transient pores in the cell membrane. Cells then exchange molecules with the surrounding medium while the transient holes are open. Sonoporation is achieved through ultrasound-driven bubble pulsations. Ultrasound exposure has been shown to be an efficient method for the transfection of bio-molecules into mammalian cells and tissues in vitro and in vivo [Liu 2003]. The ultrasound transfection process is simpler as compared to other direct delivery methods such as particle bombardment and electroporation. The primary mechanisms of sonoporation are the effects of heating and cavitation as a result of an applied ultrasound pulse. Cavitation causes mechanical perturbations of the cell membrane due to the collapse of bubbles generated by the application of the ultrasound [Liu 2003]. The magnitude of the acoustic cavitation can be further enhanced using ultrasound contrast agents (UCA) such as Levovist, Albunex or Optison [Miller 2002]. Most commercial UCA are made of gas microbubbles, and are used as cavitation nuclei which enhance the effects of the ultrasound induced cavitation and result in substantially higher molecular uptake [Miller 2002]. Microbubbles lower the threshold of energy required for cavitation. Additionally, bio-molecules may be incorporated inside or on the surface of the microbubbles such that they release and deliver them into the cells during cavitation [Liu 2003].

The principles of miniaturization have also been applied for sonoporation devices to provide single-cell transfection control. These devices have been used for the transfection of antisense oligonucleotides (ASO) [Siu 2007] and human promyelocytic

leukemia cells [Le Gac 2007], using piezoelectric induced ultrasound and laser induced cavitation, respectively. In the work presented by Siu et al, a potential pulse applied to a piezoelectric membrane resulted in the generation of the ultrasound. Alternatively, the device presented by Le Gac et al employs laser induced bubble cavitation in the cell chamber to enable trans-membrane transfer. The configurations are shown in Figure 3.

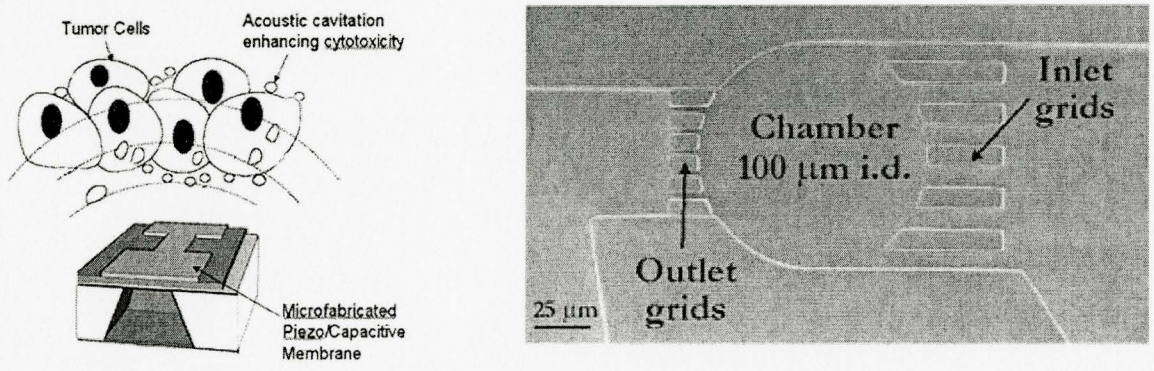

a.) b.)

Figure 3: Miniaturized sonoporation devices a.) [Siu 2007], b.) [Le Gac 2007]

If sonoporation is used to facilitate the uptake of biomolecules into cells, it is important to optimize the parameters to reduce damage to the cells and to prevent rupture and cell lysis. It features a relatively high efficiency of 43% [Mehier-Humbert 2004]. As in electroporation, the mechanisms of internalization and intracellular trafficking of exogenous molecules as a result of sonoporation have not yet been determined. However, it has been shown that the amount of internalized molecules is inversely proportional to their size, implying that the pores favor the entry of smaller more mobile species [Mehier-Humbert 2004]. This may also be due to the greater abundance of smaller pores as compared to large pores. Another similarity with electroporation is the lack of nuclear targeting. Mehier-Humbert et al showed that particles could be delivered into the cytoplasm, but not directly into the nucleus, therefore degradation of the internalized biomolecules by enzymes remains a problem [Mehier-Humbert 2005].

Another major challenge is to obtain high transfection rates with good cell viability. This is because cells are damaged or killed if the induced pores are too large to be resealed in a timely fashion. Furthermore, just as electroporation, it is also a non-quantitative delivery process and it is not possible to control the amount of material that is delivered into the cells. As a result of these limitations, sonoporation is presently not suitable for large-scale clinical testing.

2.6.4 Capillary Microinjection

In capillary microinjection transfection is achieved through the direct insertion of a microinjection needle into the cell using a microscope and micromanipulators. A typical microinjection setup is shown in Figure 4.

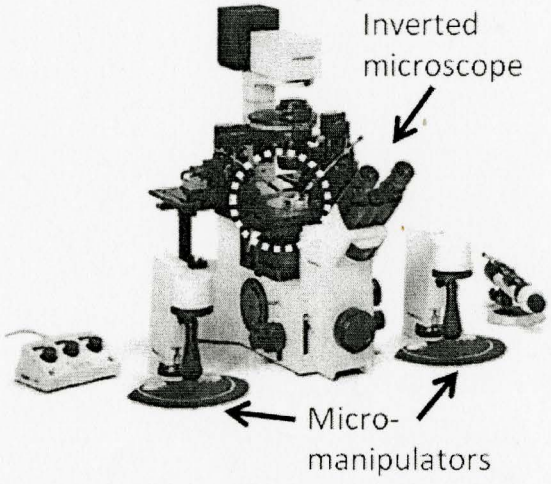

Figure 4: Microinjection setup

In the case of adherent cells only a microinjection needle is required for the injection of materials into the cell. For suspension cells a holding pipette or other means of immobilizing the cells for injection is required, as shown in Figure 5.

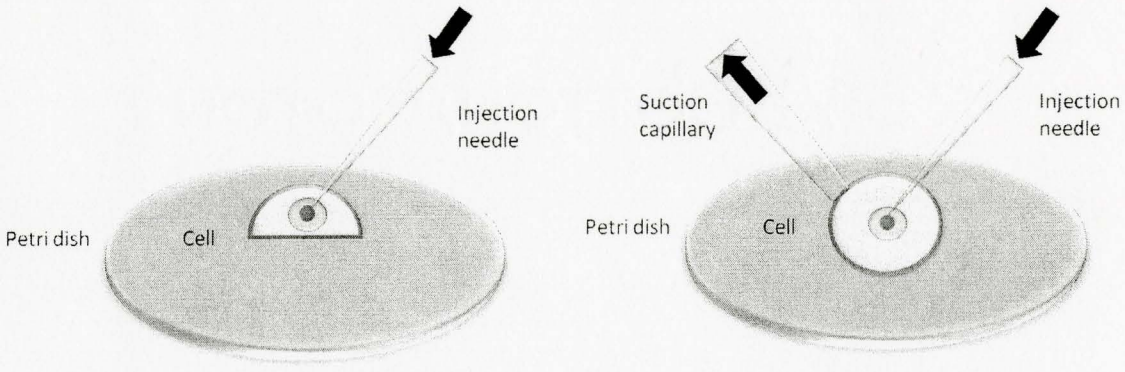

Figure 5: Suspended cell and adherent cell microinjection

Two distinct capillary microinjection techniques exist, differing in the mechanism used for reagent transport. These are capillary pressure microinjection (CPM), which uses pressure driven flow (PDF), and iontophoresis which employs electrokinetic principles (electrophoresis) for reagent transport. CPM is widely used as it is the simplest and most direct way to inject extracellular material in a quantitative and targeted fashion (cytoplasm or nucleus) without cell or reagent restrictions [Mehier-Humbert 2004]. A wide range of substances, including naked DNA, RNA, antibodies and nanoparticles have been injected into cells with high transfection efficiency (up to 100%) and low cytotoxicity [Zhang 2008]. The volume to be delivered is determined by the magnitude and length of the applied pressure pulse. However, precise volume control remains a problem and the reagent delivered into cells may vary by a factor of 5 or more, resulting in significant variability and low reproducibility [Minaschek 1989]. The use of pressure for injections imposes limitations on CPM. Smaller injection needles increase the viability of injected cells, as they reduce the damage imparted by the mechanical puncture of the plasma and nuclear membrane [Walton 1987]. However, current CPM

tools are at their limit (diameter>0.2-0.5μm) due to the high pressures needed to dose using nanoneedles which is beyond the ~500-600kPa range of commercial systems.

Iontophoresis reduces some of the limitations associated with pressure driven flow by using electrophoresis for reagent transport. It has been used for the injection of lucifer yellow into Hydractinia echinata embryos [Pfannelstiel 1985], DNA into green monkey kidney cells [Ocho 1981] and into mouse tissue cells and embryos [Lo 1983]. Electrodes are connected to the injection needle and to the cell medium to allow for the generation of the electric field necessary to enable ion transport. As this method does not employ pressure for reagent transport, it also enables the use of smaller injection needles. The flow rates for iontoporetic injection at steady state can be calculated using [Purves 1980]:

$$q = nI/zF$$

Equation 2: Iontophoretic injection flow rate

where I is the current in A, z is the charge number of the ion, F is Faraday's constant and n is the transport number. The transport number is the fraction of current that is carried by ion species under consideration, and is typically 0.1-0.4 for cations [Purves 1980]. As continuous electrical contact exists during injection, it also allows simultaneous monitoring of viability and physiological activity of the injected cells by measuring the current during injection [Storms 1998]. From the above equation it can be seen that ionophoretic flow depends only on current and on the properties of the ions and is not much affected by the pipette shape. The opposite is true for pressure injection as the release depends on pressure, tip diameter and taper angle, therefore variations between pipettes can result in significant variations in output. It is, however, independent of the

chemical properties of the reagents to be delivered. A major disadvantage of iontophoresis is the slow reagent delivery and the difficulty in quantifying the actual flow delivered to the cells due to diffusion and efflux from the pipette tip, which needs to be balanced by the application of a "retaining current" [Purves 1979].

Both aforementioned microinjection methods are laborious, low-throughput processes requiring manual single cell injections, resulting in significant variability and low reproducibility due to variations in operator skill and inevitable fatigue. This allows only for a few hundred cells transfections per experiment, making it impractical for large-scale clinical applications requiring statistically significant sample sizes. To address this issue, a number of semi [Matsuoka 2004] and fully automated microrobotic injection systems have been developed to enable rapid injection of Drosphilia [Zappe 2006] and Zebrafish [Wang 2007-1] embryos. However, these are complex standalone systems that are cost intensive and do not allow for the integration of cell processing operations.

Performing cell injection in a lab-on-a-chip format allows for the integration of pre and post-processing operations (cell sorting, testing of cell viability) [Andersson 2004], thus reducing cell damage due changes in the cell environment [Fukui 1996] while providing greater selectivity, less dead volume and automation [Mitchell 2001]. One example of early work in miniaturizing injection systems is that of Chun et al who developed a micromachined device consisting of two parts – one microarray of 5um-diameter injection capillaries and a complementary array of microchambers for immobilizing the cells [Chun 1998]. The device is shown in Figure 6. The device enables multiple parallel injections in a simplified fashion, however, the fabrication process is expensive and complex as it involves multiple steps of bonding and reactive ion etching (RIE), thus making it impractical for general use.

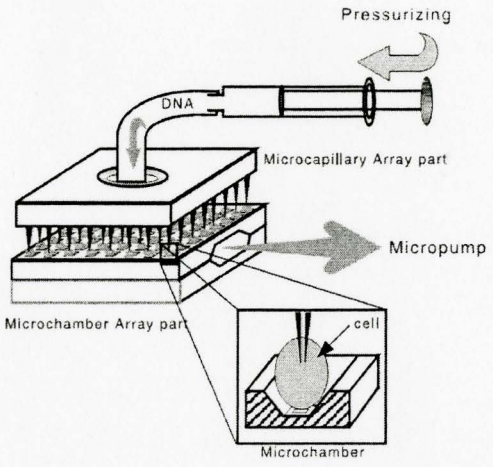

Figure 6: Microarray injection device [Chun 1998]

Another example of a system incorporating aspects of microfluidics is the work presented by Lee et al [Lee 2003]. This device integrated a PDMS valve into a microinjection needle, therefore providing precise on/off control over the flow. It allowed for controlled delivery of volumes less than 1nL. The disadvantage of this device is that it does not allow for integration of pre/post-processing. Although the injections were not performed in a microfluidic format, it is an example of the use of microfluidics in a microinjection system. The layout of the device is shown in Figure 7.

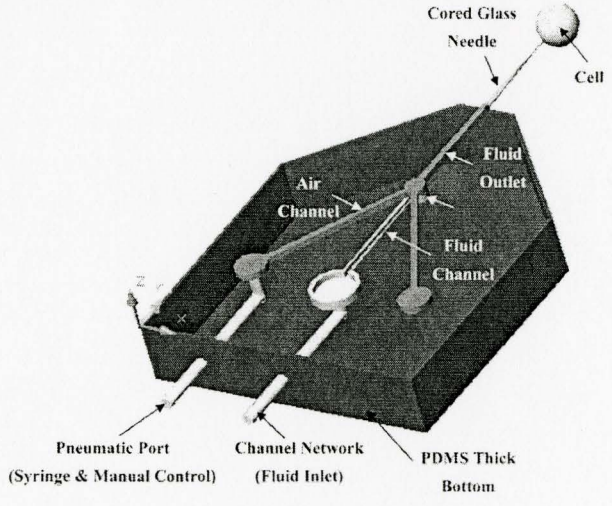

Figure 7: Micro-valve mediated microinjection control [Lee 2003]

First efforts to perform injections in a microfluidic channel were those of Hsu et al [Hsu 2004]. They presented an open-channel device which had cells cultured in it and allowed for patch clamp recordings and injections of cells with fluorescent dye. A feature of this device was that different concentrations of extracellular liquids could be flowed through the open channels and the cellular response recorded using patch clamp recordings. The device channel layout is shown in Figure 8.

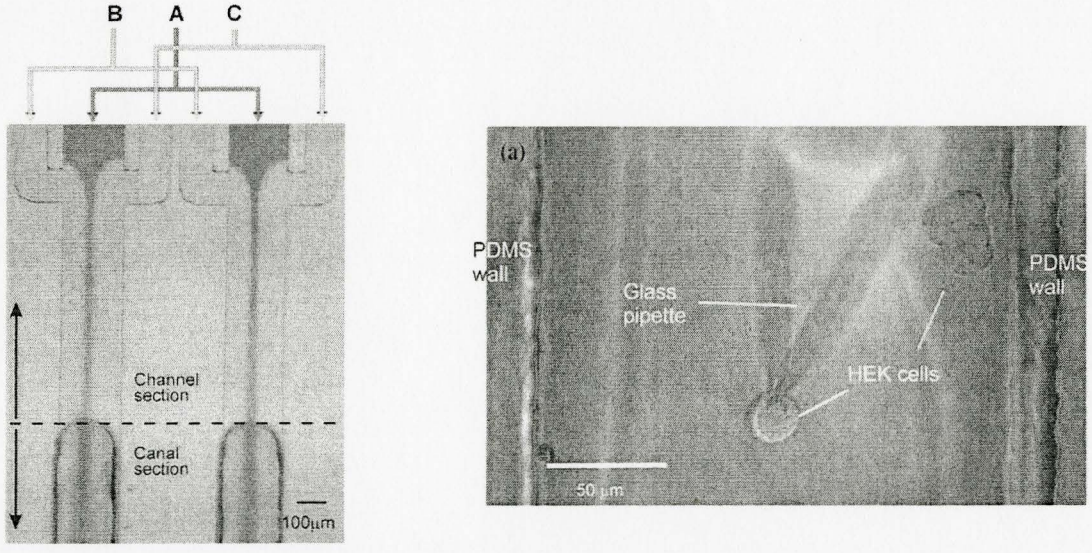

Figure 8: Layout showing closed channel section and open channel section for access for injection needle. [Hsu 2004]

Although the injections were performed in microchannels, this was not a microfluidic injection system as the injections were performed with an external microinjection needle by a trained operator. Therefore, this device could be useful for patch clamp recordings, however, does not provide any advantage for microinjections.

One device that performed injections in a microchannel is the one showed by Adamo et al. They reported a microfluidic based single cell microinjection system in which fluid flow directs a cell along a channel and onto a fixed microneedle which is connected to an external syringe pump. The cell impinges onto the needle as a result of the applied flow. The device architecture is shown in Figure 9.

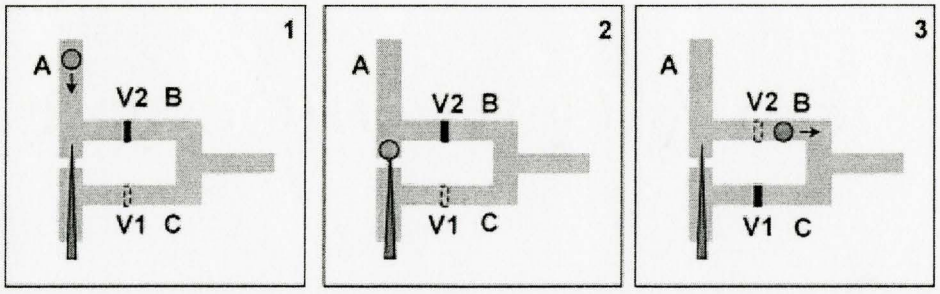

Figure 9: Microfluidic cell injection method. a.) Cell is moved by the fluid stream towards the microneedle, valve 1 (V1) is opened and valve 2 (V2) is closed. b.) The cell is pierced by the injection needle and injected. c.) V2 is opened and V1 is closed which causes a reversal of flow to lift the cell off the needle and transport it along channel B and out of the device. [Adamo 2008]

Although this device has potential to enable high-throughput injections, it has a number of disadvantages. Firstly, cells have to be sorted according by their size to ensure that they are not too large to clog the channel, or too small to be pierced and lysed by the injection needle. The device may also not work for larger cells and embryos as the fluid pressure may not be sufficient to force the needle in without causing damage to the cell. Furthermore, as the needle is fixed in place one loses the ability of targeted delivery (selectively being able to inject into the cytoplasm or nucleus). It does not allow for control of force and depth of injection. It also assumes that the cells are uniform and the nuclei are located at the exact centre. It does not allow lateral adjustment of the injection needle. Additionally, the placement of the injection needle is a very complicated process performed using a microactuator to ensure that the tip extends into the channel at a given length. It also requires a valving system to perform the injections, which will limit the performance of the device. And finally, the device relies on an external syringe pump to perform the injections and is therefore not truly in a "lab on a chip" format. Therefore, to summarize although this device does provide some advantages over the presented micro and macro injection methods, it still has a number of disadvantages which limit its use.

2.7 Summary

This chapter provided an overview of existing cell transfection methods, introduced microfluidics and microfluidics based injection systems. From the literature review it can be seen that capillary microinjection has a number of advantages over other methods. However, the problems that need to be addressed to make it viable for clinical applications are low throughput, injection variability and dosage control. Table 1 provides an overview of the various methods presented.

Table 1: Overview of injection methods (Adapted from [Mehier-Humbert 2004])

Technique	Method	Advantages	Disadvantages
Biological	Viral vectors	Very high efficiency	Non-quantitative, high cytotoxicity, high cost
Chemical	Synthetic vectors	Low to High efficiency	Non-quantitative, cytotoxicity, no nuclear targeting
Gene Gun	Particle bombardment	Medium efficiency (Up to 34%)	Limited carrying capacity, non-quantitative, cytotoxicity
Electroporation	Electric cell permeabilization	Medium efficiency (Up to 30%)	No nuclear targeting, non-quantitative, cytotoxicity
Sonoporation	Acoustic cell permeabilization	High efficiency (up to 43%)	No nuclear targeting, non-quantitative, cytotoxicity
Capillary Injection	Insertion of capillary	Very high efficiency (up to 100%), targeted delivery, low toxicity	Low-throughput, injection variability

Although automated systems have been developed for injection, these are presently limited to large embryos and are complex standalone devices that do not allow for integration of processing operations. A number of microfluidic systems have been

developed to allow high throughput injections in an integrated fashion, however these also suffer from limitations and restrictions that will prevent widespread adaptation. Additionally, they still employ pressure driven flow, which puts restrictions on microinjection needle size and volume control. Therefore, the ideal device would maintain the advantageous properties of microinjection and eliminate the issues related to throughput, variability, provide precise volume control and obviate restrictions on injection needle sizes. Our prototype device is presented in the following chapter.

CHAPTER 3
MINIATURIZED CELL INJECTION DEVICE

3.1 Introduction

As presented in the previous chapter, capillary microinjection provides a number of advantages over other methods, such as low cytotoxicity and high transfection efficiency, however throughput and variability pose a problem. Our device addresses these problems by enabling high-throughput in an integratable 'lab on a chip' format with high repeatability. This chapter introduces our device design.

3.2 Advantages over Existing Methods and Devices

Our design allows for fully integrated, potentially automated injections in a miniaturized 'Lab on a Chip' format. This provides greater control over injections and results in reduced reagent use and less dead volume. Additionally, it enables the reduction of cell damage due changes in the cell environment as the cell supply, transport and injection is done entirely on-chip [Fukui 1996]. It overcomes other limitations of traditional microinjection such as the needle tip size (dependent on maximum injection pressure), minimum reagent volume and the need for specialized pumps. This is achieved by performing reagent injection by electroosmotic flow, rather than pressure

driven flow. The use of electroosmosis for reagent injection provides a number of advantages over pressure driven flow such as the absence of moving parts, precise electrical control over flow and virtually unlimited resolution [Devasinathipathy 2003]. Additionally, our device can also be used for electrical detection of breakage or clogging of the injection needle [Lukkari 2004]. The overall system architecture is scalable to allow for miniaturization, multiple parallel injections and autonomous functionality.

3.3 Device Layout and Working Principle

The device (Figure 10) consists of a flexible PDMS polymer substrate with two separate and fully enclosed channel structures 2mm wide and 2mm deep. One channel supplies the injection targets and the other channel the reagent. For capturing and immobilizing targets, a hollow glass capillary (1mm OD, 0.5mm ID) is bonded into the 1mm wide by 1.5mm deep groove perpendicular to the target supply channel. A tapered hollow glass microneedle (10μm OD, 5μm ID tip) aligned collinear to the suction channel is used for injections.

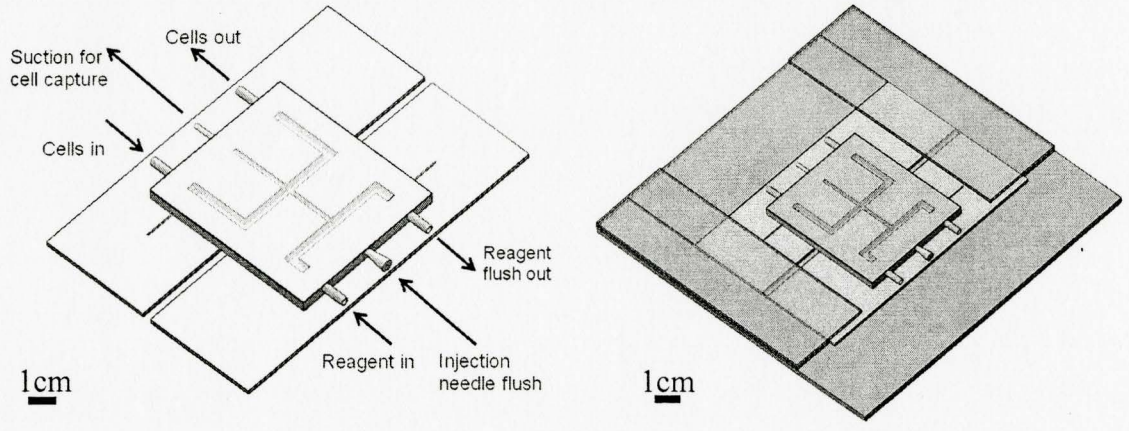

a.) b.)

Figure 10: a.) Injection device layout and b.) Device mounted in base

As the suction capillary and the injection needle base diameter are equal (1mm), the needle tip is aligned in the centre of the suction capillary when they are placed into the collinear 1mm wide channel. The open cross section of the device showing the alignment of the needle and suction capillary is shown in Figure 11.

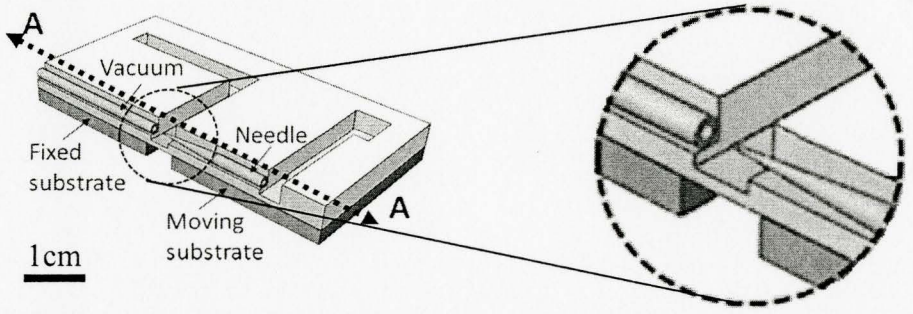

Figure 11: Open cross section of device showing suction capillary and needle

The flexible PDMS substrate is bonded onto two separate glass substrates that are aligned with the edges of the target supply channel such that all regions except for the target channel bottom are reinforced. Hollow glass capillaries (2mm OD, 1.8mm ID) coupled into the target and reagent supply channel provide inlet and outlet ports for the device. A 30 gage needle inserted into the injection needle through the back of the device (Figure 12) is used to flush the injection needle and to clear any blockage.

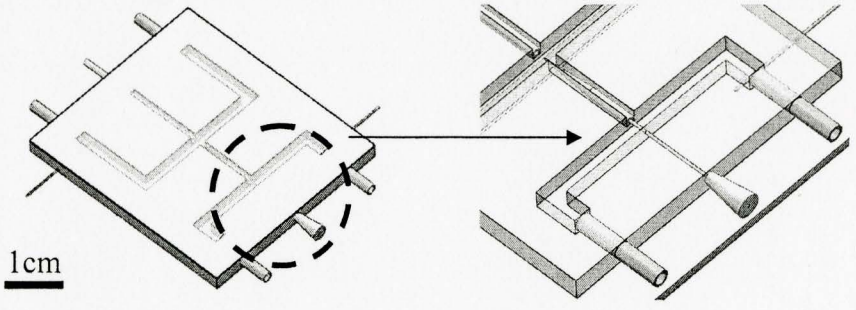

Figure 12: Loading and flushing of injection needle

The device is loaded into a base assembly which ensures that there is only longitudinal movement when a displacement is applied to the movable substrate using a linear actuator. The injection sequence is as follows, the embryos are loaded into the device using pressure driven flow. As the embryo approaches the centre of the device it is immobilized by the suction capillary which is aligned collinear to the injection needle. Subsequently, the embryo is injected by the integrated needle. The actuation of the integrated needle is achieved by the compliant and reversible deformation of the target supply channel bottom membrane. Due to the selective reinforcement of the device, the bottom of the target supply channel buckles as a result of the applied force, thus effectively causing the actuation of the needle (Figure 13).

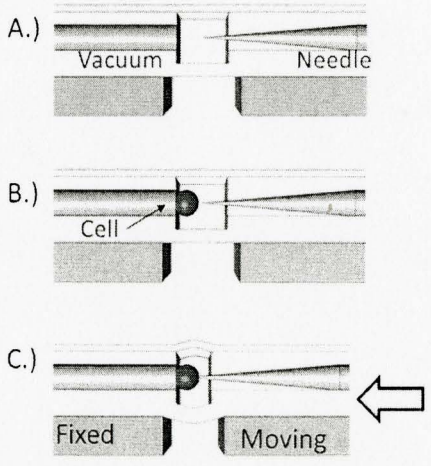

Figure 13: a.) Neutral state b.) Embryo captured c.) Embryo injected

The injection mechanism takes advantage of the flexible nature of the PDMS substrate [Noori 2008-1]. The linear displacement is applied using a Thorlabs MBT616 micropositioner block. Since the suction channel and the injection needle are aligned collinear to one another, only a single degree of freedom is required for injection. This also eliminates damage inflicted to cells due to lateral movement of the injection needle.

Furthermore, as the injection occurs in a planar configuration it provides precise control over the microinjection location (cytoplasm or nucleus). This injection mechanism greatly reduces complexity and variability associated with microinjection and eliminates the requirement of trained operators, as it obviates the need for complex micropositioners and can be fully automated. Once the needle has been injected into the cell, the pumping of the reagent into the cell can commence.

3.3.1 Cell Loading, Transport and Immobilization

The schematic for the cell loading process is shown in Figure 14. The cells are visually located in a Petri dish and loaded into the device by bringing the tube connecting to the inlet port of the target supply channel close to it and applying suction to the outlet port of the target channel using a syringe.

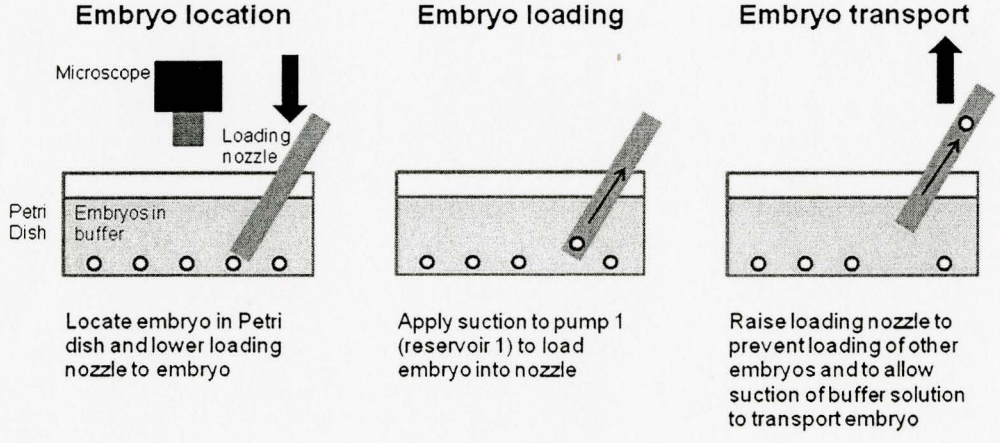

Figure 14: Embryo loading process

Although loading is presently done manually, this process lends itself to automation using optical feedback. Once a cell has been loaded, the tube is raised to prevent further cells from being sucked in, while providing uninterrupted flow of the buffer medium.

After the cell has been injected it is transported to the syringe reservoir. A major advantage of this approach is that the cell never leaves its original buffer environment, thus reducing environmental shocks experienced by the cell which can greatly affect cell viability [Fukui 1996]. Loading can proceed in a continuous fashion with predetermined spacing between each loaded cell. This enables rapid loading and processing of cells. As the loaded cell nears the injection site, transport is ceased and negative pressure is applied to the suction channel to capture the cell for injection. This effectively immobilizes the cell in perfect alignment to the injection needle. Detection of the presence of an immobilized cell can easily be automated using optical means or by sensing pressure change in the suction capillary due to cell presence. Injection can proceed once a cell has been immobilized by the suction channel. After the embryo has been injected, the suction is released and a pulse of positive pressure is applied to release the embryo from the capillary. The embryo is then transported in the channel by again applying suction to the syringe connected to the outlet channel of the target supply channel. Presently, a 50mL syringe acts as the final reservoir for the injected embryos. Once the injections are completed the embryos stored in the syringe can be released into a petri dish.

3.3.2 Electroosmotic Reagent Transport

The pumping of the reagent through the needle and into the cell is performed by electroosmotic flow induced by a potential applied to electrodes embedded in the target and reagent supply channels. The electrodes are inserted into the channels and create electrical contact with the solution inside the channels. This generates an electric field across the injection needle and induces the electro-osmotic flow of the liquid in the needle. The schematic of the path of the potential is shown in Figure 15.

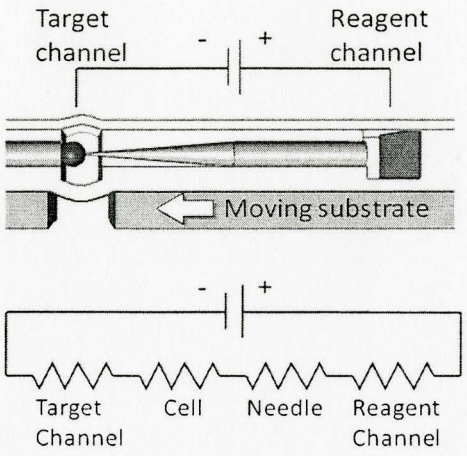

Figure 15: Path of potential in injection device

Electroosmosis is defined as the motion of an electrolytic solution caused by the application of an electric field [Devasinathipathy 2003]. This motion is possible as a result of the spontaneous formation of an electric double layer due to the surface charges at the interface of a surface and a liquid. In the case of glass, it acquires a negative charge upon exposure to an electrolyte due to deprotonation of silanol groups Figure 16.

$$SiOH <=> SiO^- + H^+$$

Figure 16: Deprotonation of silanol groups on surface of glass

The negative surface charge causes the formation of a positive Stern layer which consists of counterions which bond to the charged surface. This is shown in Figure 17. Adjacent to the Stern layer is the Gouy-Chapman layer which consists of a layer with a net positive charge due to the attraction of positive ions and repulsion of negative ions by the negatively charged surface. The line of separation between the Stern layer and Gouy-Chapman layer is the shear plane along which the flow will occur.

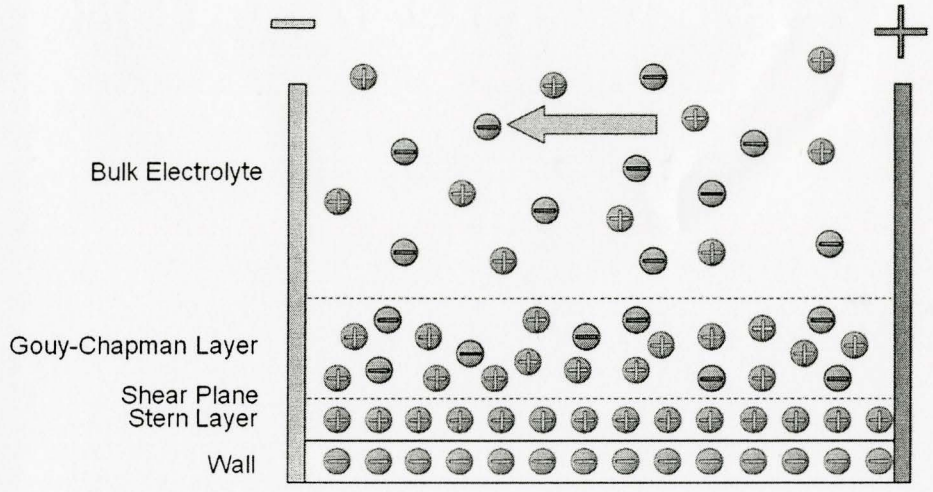

Figure 17: Formation of electric double layer due to negative surface charge

The Stern layer is a layer of immobile positive ions which are strongly bonded to the negatively charged surface of the wall. Adjacent to it is the layer with a layer of ions with a net positive charge. When a potential difference is applied along the length of the channel this induces the bulk movement of the liquid from the positive potential towards the negative potential, which moves over the shear plane which separates Stern layer from the Gouy-Chapman layer. This is because the Gouy-Chapman layer is attracted towards the negative potential because of its net positive charge and thus drags the bulk liquid with it. The phenomenon is governed by the Smoluchowski-Helmholtz equation which is derived from the Navier-Stokes equation and assumes that the electric double layer is small compared to the diameter of the channel. The equation is given below, for derivation refer to [Rice 1965].

$$u_{eo} = \mu_{eo} \cdot E_z$$

$$\mu_{eo} = \frac{\epsilon \cdot \zeta}{\eta}$$

Equation 3: Flow induced by electroosmosis (Smoluchowski-Helmholtz equation)

The first equation is electroosmotic velocity, consisting of μ_{eo} which is the electroosmotic mobility, and E_z which is the electric field collinear to the channel. In the electroosmotic mobility, ϵ denotes the dielectric constant, ζ is the electrokinetic or Zeta potential which denotes the potential difference across the electric double layer, and η which is the fluid viscosity. A major advantage of electroosmotic flow is that it provides a non-pulsating steady plug-like flow (Figure 18) and thus allows for precise dosage control with sub-picoliter flow rates with reduced reagent dispersion.

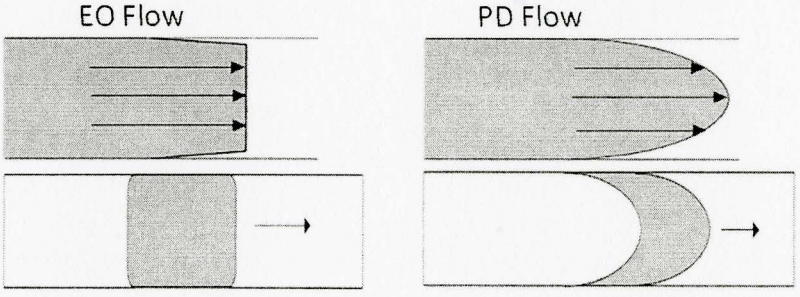

Figure 18: Flow profile of EO vs. PD flow

Using electroosmosis for reagent transport provides full scalability for the reagent pumping mechanism as it obviates the restrictions on needle size (d>0.2μm) due to pressure limitations of existing injection systems.

3.3.3 Detection of Clogged or Broken Needles

An advantage of having integrated electrodes is that it allows for automated detection of clogging and needle breakage. Detection of clogging or damage to injection needles presents a challenge in convential microinjection. If clogging is not detected, it may result in variability in reagent volume or no reagent being delivered at all during injections [Kallio 2006]. Clogging may be detected visually, however this does not

provide a quantitative measurement of the extent of the problem. Chipped or broken needle tips may also go unnoticed. Therefore, to obtain consistent and reproducible results it is necessary to have an efficient detection method. This can be done by measuring the resulting change in resistance across the injection [Lukkari 2004]. During device characterization it was found that needle breakage resulted in a decrease in the resistance, whereas clogging caused the resistance to increase. This method allows for the continuous monitoring of the needle state. Furthermore, it can be used to detect the contact between the needle tip and the cell, thus providing a feedback mechanism, in addition to visual detection, to enable full automation of the injection process. A summary of the injection process flow is shown in Figure 19.

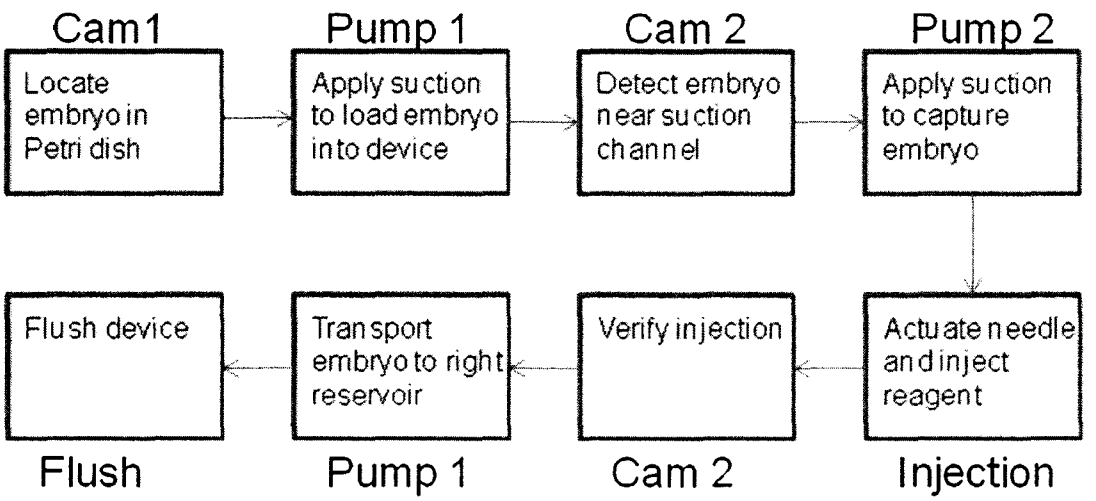

Figure 19: Injection process flow

For the detailed setup and proposed algorithm for full automation and post processing refer to Appendix B.

3.4 Device Design Criteria and Parameters

The determining factor for the design of the device was the ability to inject Xenopus Laevis eggs and Zebrafish embryos in a high-throughput fashion. This determined the size of the channels, the size of the suction capillary used to immobilize the embryos and the size of the injection needle. These parameters are discussed in further detail below.

3.4.1 Channel Geometry and Size

In order to accommodate the ~1mm diameter eggs and embryos, the channels were designed to be 2mm square. This ensures the uninterrupted transport of the embryos in the device. Furthermore, it allows the injection needle to extend approximately 1mm into the channel, and thus provide the capability to inject into any location in the immobilized Zebrafish embryo. The channels that hold the injection needle and the suction capillary were 1mm wide to allow for these components to be bonded and sealed in place.

3.4.2 Vacuum Channel Dimensions

The borosilicate suction capillary that was used had a 1mm outer diameter and 0.5mm inner diameter. This particular size was chosen as it provided enough suction to immobilize the Zebrafish embryos and the Xenopus Laevis eggs without causing them to be sucked into the capillary. Furthermore, it enabled immobilization with no visible damage to the eggs and embryos.

3.4.3 Injection Needle Size

The injection needles were fabricated from stock borosilicate tubes with 1mm outer diameter and 0.5mm outer diameter. This ensured that when the needle and the capillary were aligned into the 1mm channels they would be collinear to one another. The needles were fabricated using a Sutter P97 micropipette puller, with specific settings that ensured

a long uniform taper. The long uniform taper was used as it results in reduced damage to the eggs and embryos upon insertion. The tip diameters used for the device were between 10 and 20 micrometers. This range of dimensions was used as it ensured mechanical stability of the needle and was also used in the literature to result in viable Zebrafish embryo injections [Wang 2007].

3.5 Design Iterations

The device went through a number of design iterations. There are a total of 5 prototype designs that were fabricated and tested. The initial prototype was merely a proof of concept to determine whether PDMS molds fabricated using a polymer printer could be used for our purposes. This initial prototype 1 was then reduced in size to obtain prototype 2, which was tested and characterized for the compliant mechanism and the electroosmotic pumping. This prototype was further miniaturized to obtain prototype 3, which was still an open configuration. The next prototype 4 was a fully enclosed device which allowed for the reagent and target supply to be performed using pressure driven flow. The device featured vertical supply channels which were used to introduce materials into the target and reagent channels. However, this posed a number of problems as this induced pressure imbalances due to hydrostatic pressures in the tube. To amend this, the final prototype was created, prototype 5, which features horizontal supply channels, which effectively eliminate problems of hydrostatic pressures. The devices are shown in Figure 20 a.)-d.).

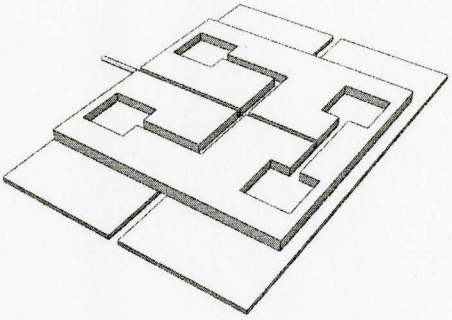

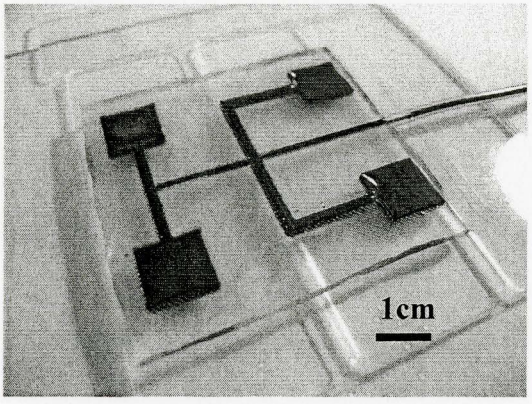

a.)

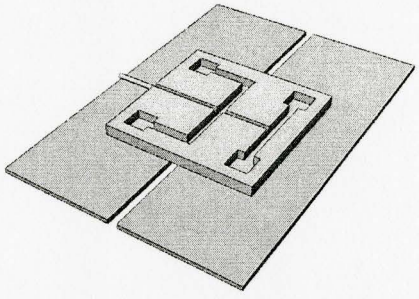

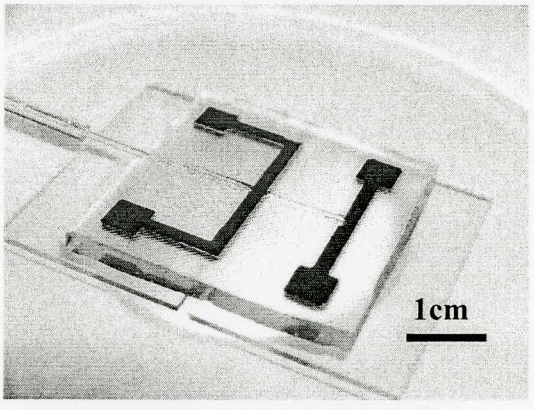

b.)

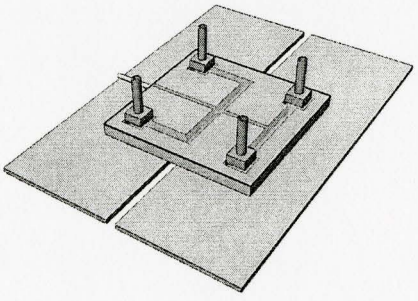

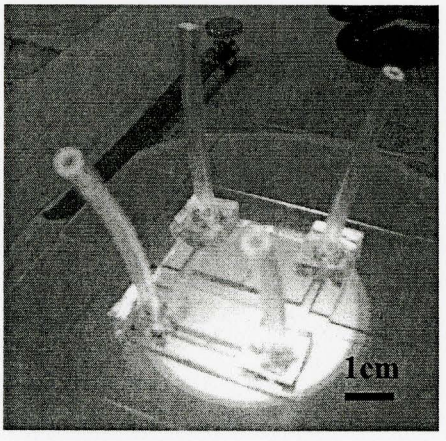

c.)

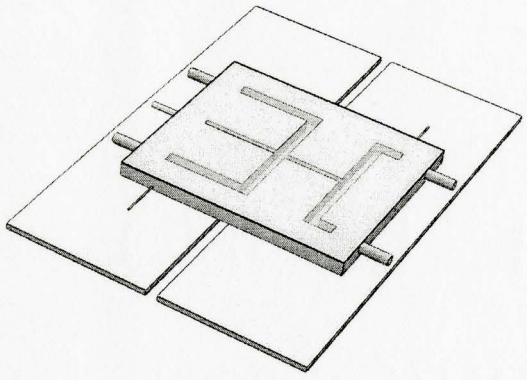

d.)

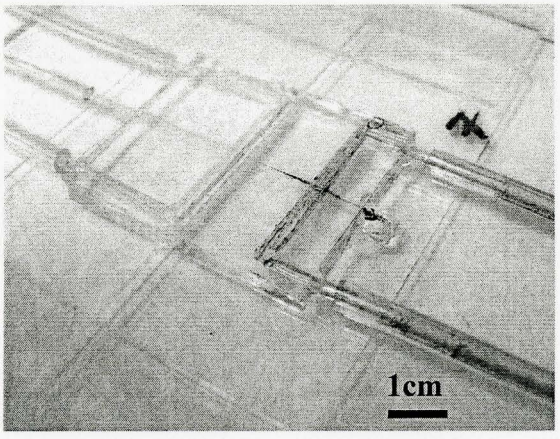

Figure 20: a.) to d.) Prototypes 2, 3, 4 and 5, respectively

3.6 Summary

This chapter introduced our proposed device, its working principles and advantages over existing devices and methods. The device overall maintains the advantages of capillary microinjection such as high transfection efficiency and low cytotoxicity, while eliminating the problems associated with low throughput and dosing problems caused by pressure driven flow. Additionally, it provides the capability to detect broken or clogged needle. The next chapter will focus on the fabrication of the device.

CHAPTER 4
DEVICE FABRICATION

4.1 Introduction

This chapter introduces the fabrication techniques and materials used in the assembly of the device. The process of fabricating 'lab on a chip' devices generally starts with a technical drawing which can be made with modelling software such as SolidWorks or Autodesk Inventor. Once the design is completed, it is used to generate a master mold for the fabrication of the final device. The process flow is shown in Figure 21.

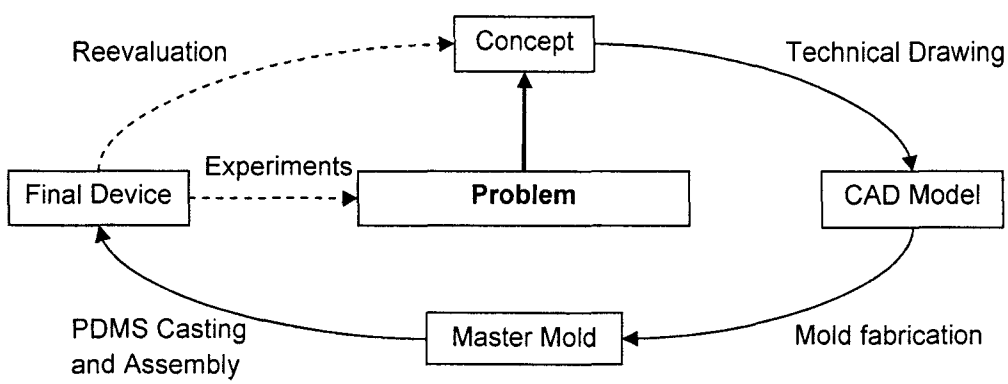

Figure 21: Process flow for device fabrication

Once the master mold is fabricated, a negative impression can be generated from it by

casting or spin-coating a polymer onto the mold. For our device we used the silicon-based polymer PDMS (poly dimethylsiloxane) to generate the building blocks of the final device [Cooper 2002]. Once the device is fully assembled, it goes through an iterative process of characterization, evaluation and redesign, if necessary.

4.2 Materials

4.2.1 ABS (Acrylonitrile butadiene styrene)

In our fabrication we used ABS molds. Acrylonitrile butadiene styrene (ABS) is a thermoplastic alloy used in the fabrication of molded products. It is derived from a combination of acrylonitrile, butadiene, and styrene [Parker 1997]. Acrylonitrile is a monomer produced from propylene and ammonia, butadiene is produced from butane and the monomer styrene is derived from coal. Their chemical structures are shown in Figure 22. The ABS alloy is light and rigid, and provides high resistance and toughness. ABS polymers are chemically resistant to aqueous acids, alkalis and alcohols. This makes the material well-suited as a reusable mold for soft lithography.

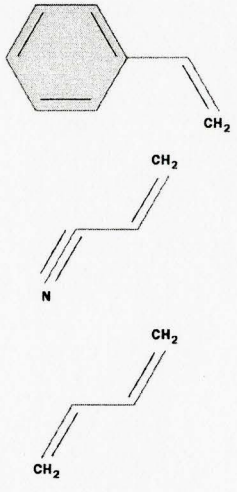

Figure 22: Monomers used in ABS: styrene, acrylonitrile, 1-3-butadiene

4.2.2 Parylene

Parylene is the commercial designation of a class of polymers called poly para-xylenes [Noori 2008]. Three forms of Parylene are commercially available in stable dimer forms, these include Parylene N, Parylene C and Parylene D (Figure 23). They are variations of a basic xylylene Parylene N polymer with the substitution of the aromatic hydrogens with one Chlorine molecule for Parylene C and two Chlorine molecules for Parylene D. These Parylene polymers are deposited by chemical vapor deposition in a vacuum and polymerized in-situ. This allows for the deposition of uniform conformal thin films.

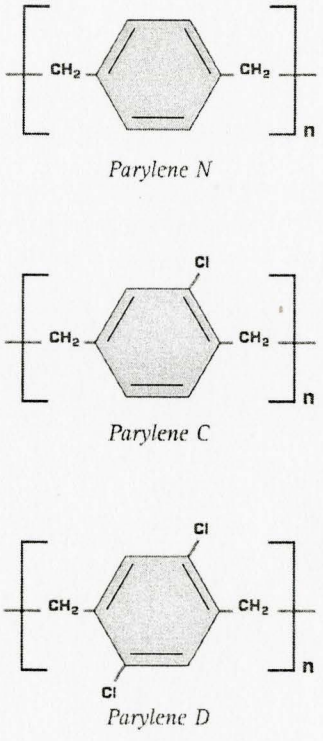

Figure 23: Chemical structure of parylene varieties [Noori 2008]

Parylene films feature low surface roughness, pinhole free coating, and excellent dielectric breakdown characteristics. The polymerization occurs at room temperature so

they are free of residual stress, chemically and biologically inert, and resistant to acids and bases. They also provide excellent surface passivation capabilities, therefore enabling the deposition and peeling of very thin PDMS membranes (>150 μm) from silicon wafers, which would not be possible without parylene treatment

4.2.3 PDMS (poly dimethysiloxane)

PDMS is a silicon-based organic polymer, also referred to as Sylgard 184, and is widely used for the fabrication of microfluidic and 'lab on a chip' devices [Cooper 2002]. PDMS is a two part resin system containing vinyl groups and hydrosiloxane groups.

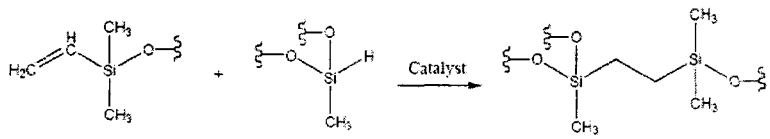

Figure 24: Cross-linking of PDMS

Mixing the two resin components together leads to a cross-linked network of dimethylsiloxane groups, as seen in Figure 24. After mixing and curing, it turns into a transparent, flexible material with a Young's modulus around 750kPa. PDMS is inexpensive, optically clear and non-toxic and it is possible to use it to fabricate complex multilayer structures. Many components such as pumps, valves and mixers have been created in PDMS [Cooper 2002].

4.2.4 Borosilicate (Corning 7740)

Borosilicate glass is a heat-resistant glass developed in the late 19th century, consisting of a combination of boron, silicate sand, soda, and ground lime [Noori 2008]. The microinjection capillaries used for our device were fabricated from borosilicate capillaries using a micropipette puller. Borosilicate softens at 825 degrees Celsius and

maintains a constant ratio of inside diameter to outside diameter as it is pulled. This allows for the fabrication of a variety of different shapes and tapers. It features good chemical properties and is highly resistant to chemical attacks by water, neutral and acidic salt solutions, strong acids and organic substances. The combination of durability, chemical and heat resistance has led to borosilicate being widely used for biological and chemical laboratory equipment.

4.3 Soft Lithography

Soft lithography refers to the process of fabricating structures using elastomeric stamps and molds [Cooper 2008]. For our device we used PDMS to make the fluidic molds by casting into ABS molds. The process flow for this is shown in Figure 25.

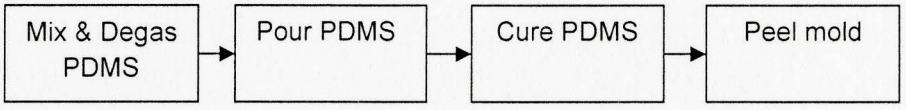

Figure 25: Process flow for PDMS

Because this material is flexible, it can be peeled from the master mold after it is cured, leaving the master intact and ready to produce another device. This is shown in Figure 26. The feature height in the PDMS is dependent on the height of the structure on which it is cast upon. The peeled PDMS layer can be bonded to another PDMS structure or a glass substrate for further processing.

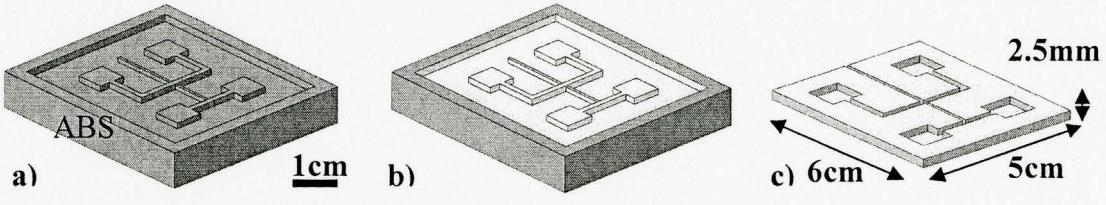

Figure 26: PDMS rapid prototyping a) ABS mold from 3D printer b) PDMS cast into mold c) PDMS peeled from Mold

The base mold used in the soft lithography process is fabricated using a Dimension BST 768 3D printer. The mold design is performed in SolidWorks modeling software and subsequently exported to an STL file format which is fed into the rapid prototyping machine. The printer imports the STL files and outputs high-quality ABS parts with a maximum size of 8x8x12in and feature resolution of 0.010in. Given that the features in our device are relatively large (≥1mm) this method is more than sufficient for our device. The channel structures are fabricated on a 1cm base and surrounded by a 2.5cm wall. The purpose of the wall is to facilitate the casting of PDMS into the mold and to provide control over the thickness of the final PDMS device. This is achieved by placing the ABS mold onto a leveling table and slowly casting the pre-polymer PDMS solution into the mold. By pouring a measured amount of PDMS until it reaches the top edge of the surrounding wall structure it is possible to achieve the required thickness for the PDMS device. In our case, the channel height was 2cm and the required channel bottom thickness was 0.5cm, therefore the surrounding walls were dimensioned to be 2.5mm tall.

The advantage of this approach is that it allows for very rapid fabrication of large and high-aspect-ratio molds for use in soft lithography in less than an hour. This compares favorably to mold fabrication using SU8 lithography, which would require a multi-layer process to achieve the aspect ratios required for our device.

4.4 Device Assembly

The assembly process for the device starts with the casting and peeling of the PDMS substrate from the ABS mold. The mold is bonded onto two separate microscope glass slides which are squared and aligned with a 2mm gap between them (Figure 27).

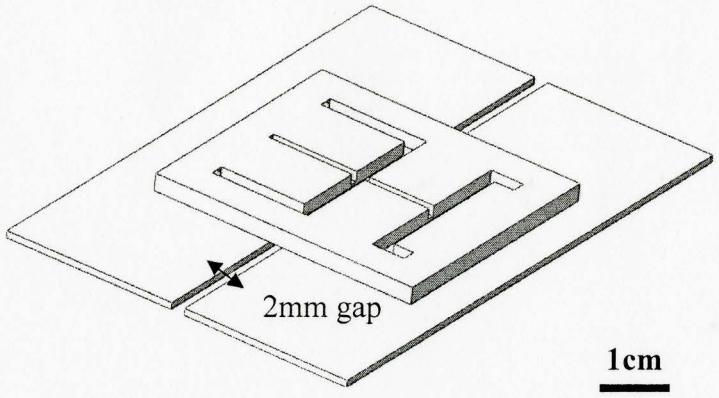

Figure 27: PDMS substrate selectively bonded onto glass slides

The PDMS mold is bonded using PDMS pre-polymer onto the glass substrates, such that all areas except for the bottom of the cell supply channel are reinforced by the glass. Subsequently, a 1mm OD/0.5mm ID borosilicate capillary is bonded and sealed into a 1mm square channel aligned perpendicular to the cell supply channel such that its face is flush with the channel side wall. A borosilicate microinjection pipette is embedded into a ridge collinear to the borosilicate capillary. The schematic for the assembly of the injection needle and the suction capillary into the PDMS mold is shown in Figure 28. The needle is aligned such that it extends 1mm into the channel. An image of the device is taken using a trinocular microscope and the diameter of the injection needle is measured, using the diameter of the suction capillary as the reference. If the tip is too small (<10um), another measurement is taken further down the taper to obtain a diameter of ~10um. The needle tip is then cleaved using needle-tip tweezers at the location of the taper which would yield a ~10um diameter tip. The needle placement is readjusted to extend 1mm into the target channel, after which it is sealed into place by the deposition of pre-polymer PDMS.

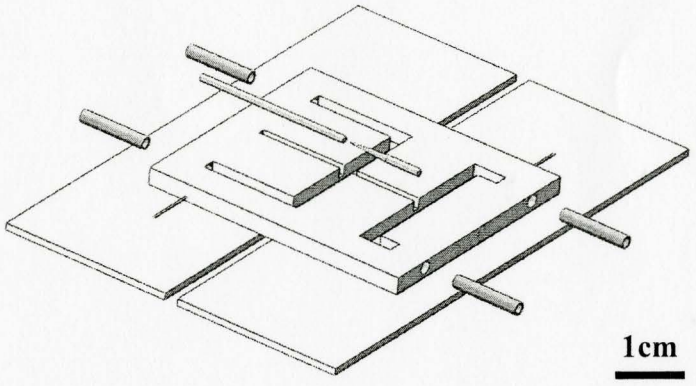

Figure 28: Insertion of suction capillary, injection needle and interconnect ports

The microinjection needles required for the device were fabricated using a standard Sutter P97 micropipette puller which has the capability to fabricate needles with diameters down to a hundred nanometers. This is more than sufficient for our purposes. Hollow borosilicate capillaries with 1mm outer diameter and 0.5mm inner diameter are loaded into the micropipette puller, passed through a heating filament and fixed onto metal clamps on both sides. The filament is gradually heated and the metal clamps apply a force to pull the borosilicate capillary as it is being melted by the heated filament. By adjusting the heat, pull force, pull velocity, time and pressure, a number of different tip sizes and tapers can be obtained. As the borosilicate capillary and the microinjection capillary have the same original outer diameter, the microinjection needle tip is collinear to the opening of the borosilicate capillary when it is bonded into place.

To provide inlet and outlet ports for the cell supply and reagent supply channel, glass capillaries with 2mm OD and 1.8mm ID are inserted into holes punched through the ends of the channels. All capillaries are sealed and bonded into place by the deposition of pre-polymer PDMS. Needle tips are inserted into the channels for electrical contact. The device is placed onto a hotplate at 65C for 15 minutes to allow the PDMS solution to harden and fully cure. Subsequently, the device is fully sealed using a 150um thick PDMS membrane, as shown in Figure 29.

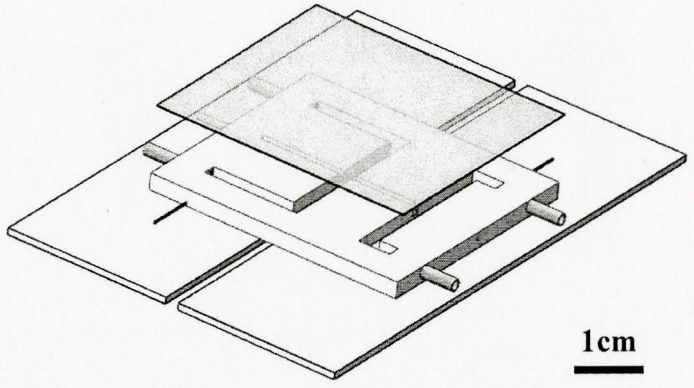

Figure 29: Bonding of membrane to enclose device

The membrane was fabricated by spin-casting PDMS onto a silicon wafer which was coated with parylene. The parylene acts to facilitate the peeling of the thin PDMS membrane from the silicon wafer. Prior to fabricating the final PDMS membrane, it was necessary to characterize the spin casting process to ensure precise control over the thickness of the membrane. This was done by spin casting a 1:30 volumetric ratio of curing agent to polymer base for 60 seconds at different speeds. The PDMS membranes were cured at 95C for 15 minutes, peeled and cut, and the cross section was measured using a scanning electron microscope. The curve fitted results are shown in Figure 30.

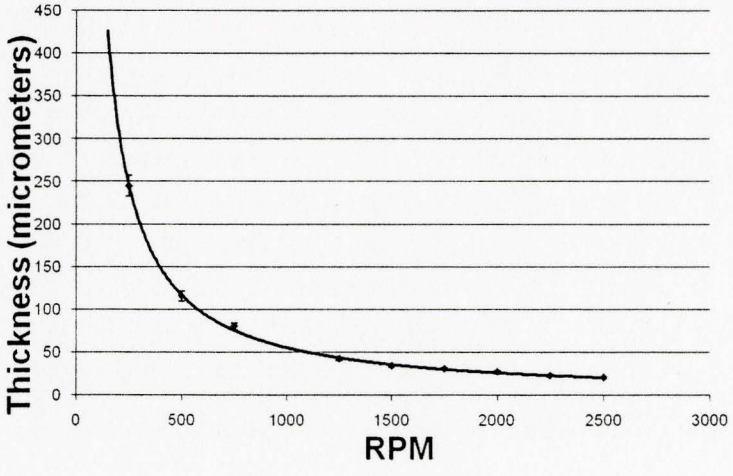

Figure 30: PDMS 1:30 spin curve

The final membrane thickness of 150um was chosen as it provided optical clarity during buckling but also allowed the peeling of the membrane from the parylene-coated silicon wafer without tearing. The membrane is bonded onto the device by first evenly depositing 1:30 volumetric ratio of pre-polymer PDMS on the device, and then slowly rolling the 150um PDMS membrane onto the device. This was done carefully to prevent air bubbles from being trapped beneath the membrane.

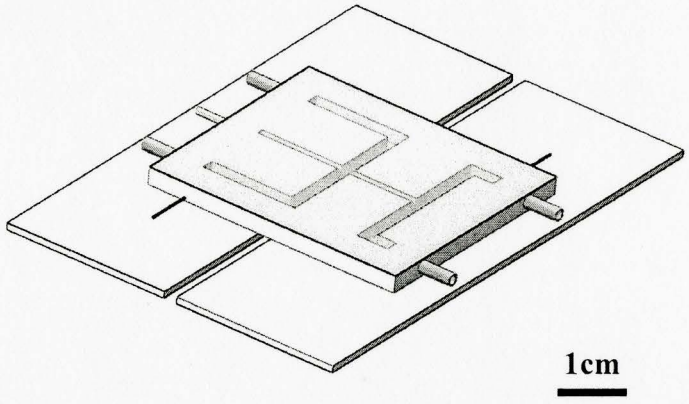

Figure 31: Assembled fluidic device

Once the device is fully assembled and cured (Figure 31), tygon tubing is connected to the inlets and outlet by interference fits. The tubing is connected to syringes which supply the reagents and the cells. The completed device is mounted into a base, which ensures that the actuation of the needle is entirely along the longitudinal direction.

4.5 Base Assembly

To ensure precise axial movement for the device, it is mounted onto a base assembly which constricts the movement of the device. To allow for visual clarity, the base is assembled using glass substrates. The supporting structure consists of a 4x4in glass substrate that is 0.25in thick. Standard 1inx3in laboratory glass slides are arranged and bonded using PDMS pre-polymer, as shown in Figure 32.

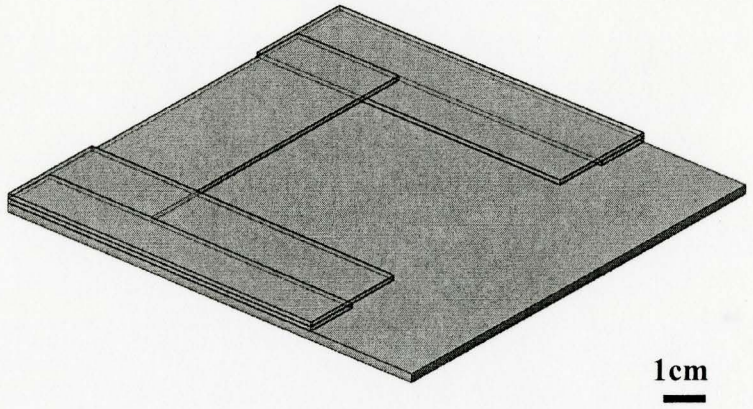

Figure 32: Fluidic device base assembly

The final assembly, shown in Figure 33, allows for the injection device to be slid in and one of the substrates to be fixed. The only component that can be actuated is the movable substrate, and as it is selectively constrained by the base assembly, it ensures that it can only be actuated linearly in one direction. This ensures precise longitudinal movement of the needle as a result of a displacement applied to the movable substrate.

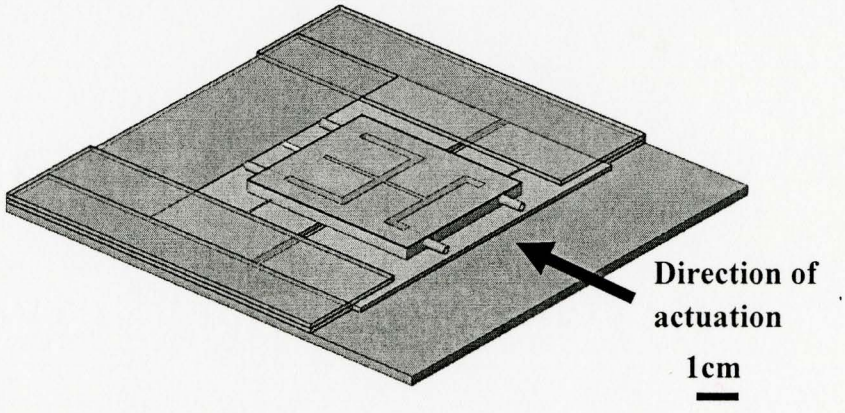

Figure 33: Injection device mounted into base

The assembled device is placed under a trinocular microscope for visualization and characterization and interfaced with a micro-positioner block to allow for the actuation of the movable substrate. The glass base is fixed onto the microscope surface using double-sided adhesive tape.

4.6 Final Device

The final assembled prototype 5 device with the interconnections for the cell supply and reagent supply is shown in Figure 34.

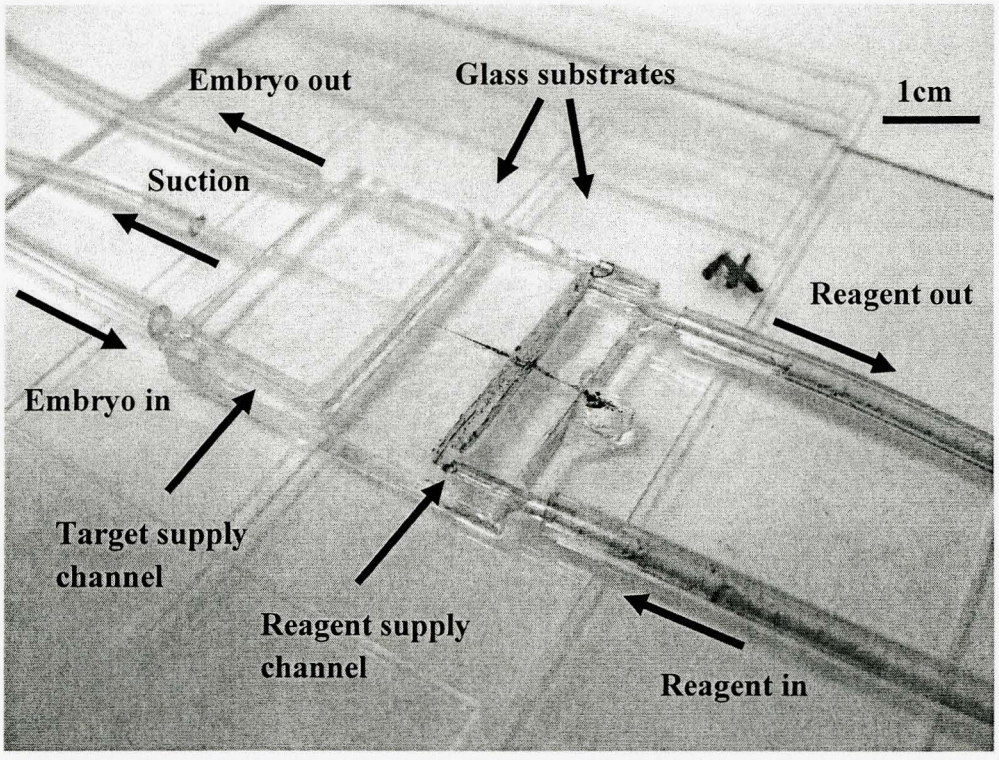

Figure 34: Final assembled prototype 5 device

4.7 Biological Samples

For our injection experiments we used Xenopus Laevis eggs and Zebrafish (Danio rerio) embryos both with ~1mm diameter. The Xenopus Laevis frog is a popular model organism which was initially used in pregnancy tests in the 1950s. They are widely

studied in cell, molecular and developmental biology as they are commercially available easily maintained and have high resistance to disease [Ny 2005]. Additionally, they live up to 10 years and can be induced to ovulate several thousand eggs up to 4 times annually [Ny 2005]. Zebrafish embryos are also widely used as model organisms for developmental studies, toxicology, toxicopathology, genetic engineering and drug discovery [Spitsbergen 2003]. The Zebrafish provides a number of advantages such as short reproductive cycle and easy maintenance. Furthermore, the embryos are transparent, which allows for observation and analysis from the beginning of fertilization. Additionally, there is strong conservation to humans both anatomically and genetically. This allows their use for modeling of complex human developmental processes, including processes involved in the generation of the kidney, heart, and hematopoietic cells [Spitsbergen 2003].

4.8 Summary

This chapter gave an overview of the materials used in the fabrication of the device, as well as the fabrication process. The fabrication process generally followed traditional soft lithography techniques, just deviating slightly in the mold fabrication process. The next chapter covers the characterization and testing of the device.

CHAPTER 5
DEVICE CHARACTERIZATION AND RESULTS

5.1 Introduction

This chapter introduces the characterization of the device and presents the results obtained. The focus of characterization was the compliant mechanism and the electroosmotic flow as these components form the foundation of the injection device. The chapter presents the results obtained, namely the injection of Xenopus Laevis eggs and Zebrafish embryos.

5.2 Experimental Setup

To enable testing, the device base is mounted and bonded onto the viewing surface of a Zoommaster 65 trinocular microscope using double-sided adhesive tape. A Thorlabs MBT616 micro-actuator block is use to apply the required displacement to actuate the device. The displacement is transferred to the device by a microscope slide that is fixed onto the surface of the micro actuator. This allows for the actuation and simultaneous imaging of the device. A Nikon 12MP digital camera connected to the microscope is used for imaging and video capture. The potential that is required for the electroosmotic flow is applied using a Keithley 2410 power source. The experimental setup is shown in Figure 35.

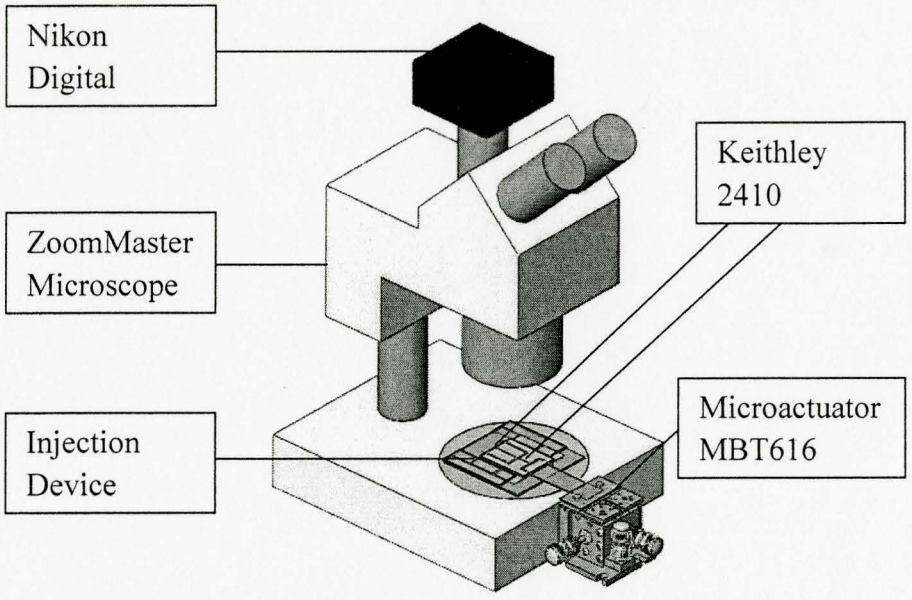

Figure 35: Experimental setup

5.3 Characterization

5.3.1 Needle Actuation

The effective actuation of the needle that is caused by the applied linear displacement was characterized for prototype 5 to provide precise control over the location of the injection inside the cell. This was done by applying a known displacement to the movable substrate and measuring the position of the needle tip relative to the suction capillary from digital images. The displacement from the microactuator block is translated to the device using a microscope slide that is mounted and fixed onto the surface of the actuator. A close-up is shown in Figure 36.

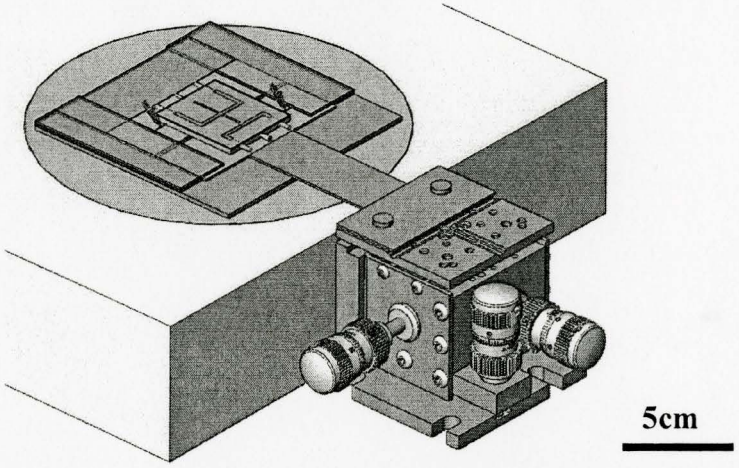

Figure 36: Microactuator connected to movable substrate using microscope slide

The displacement was applied using the microactuator and images were processed using UTHSCSA Image Tool software. The displacement of the needle as a result of the applied displacement was measured. The measured values, shown in Figure 37, showed that the needle displacement is 83.8% +/- 2% of the displacement applied to the movable glass substrate. The simulations corresponded very well to the experimental results.

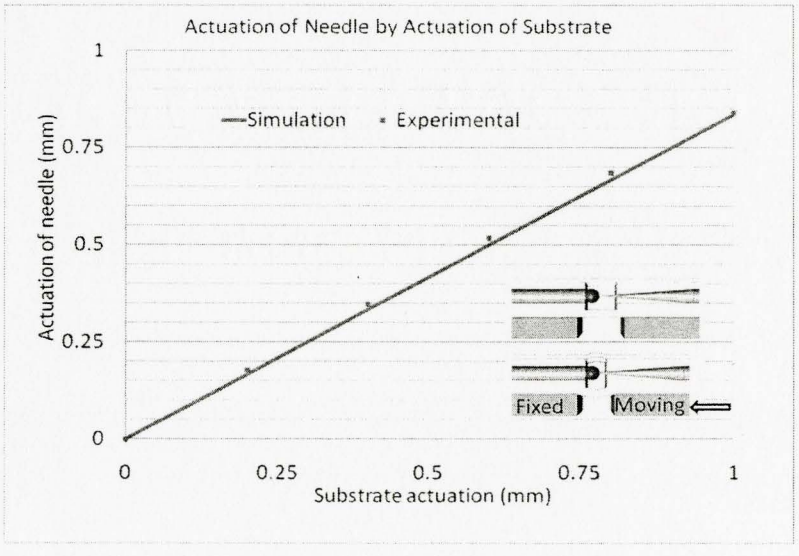

Figure 37: Actuation of needle by actuation of substrate for prototype 5

The nature of the compliant mechanism was investigated further by performing finite element simulations using CosmosWorks (Figure 38).

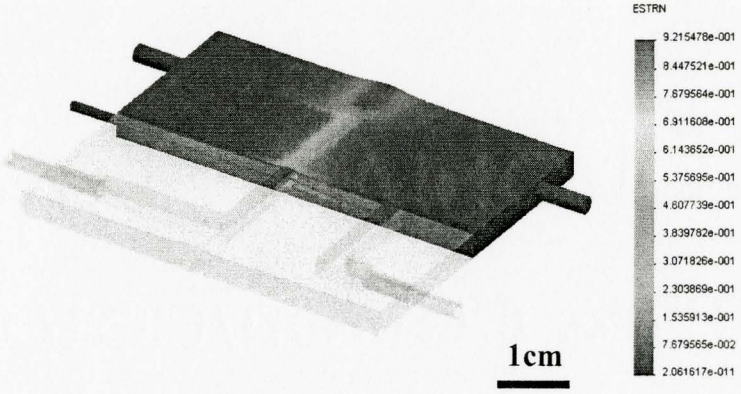

Figure 38: Strain plot of the device

A closeup of the strain plot at the centre of the device, as shown in Figure 39, shows strain imparted in regions other than the channel bottom membrane. This expected as the flexible nature of PDMS results in reaction forces causing strain in the regions adjacent to the target channel bottom. This leads to a reduction in the effective displacement of the needle by the actuation of the movable substrate.

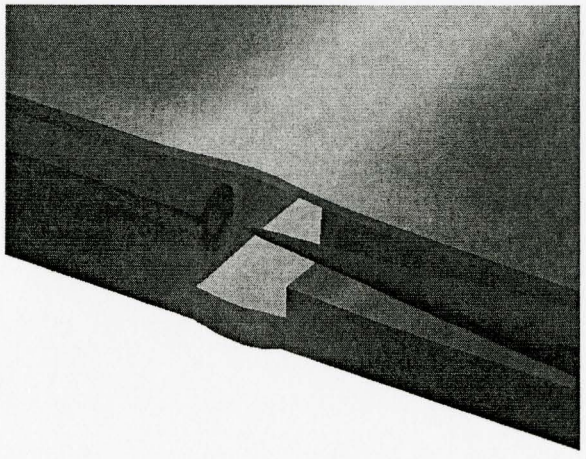

Figure 39: Reaction forces cause strain in regions adjacent to bottom membrane

As the simulations corresponded well to the experimental data, further simulations were conducted to determine the relationship between the geometric parameters and the needle actuation. The variables that were varied were the target channel bottom wall, the length of the compliant target channel and the lateral distance between the channel and the device edge and the thickness of the top membrane. These are shown in Figure 40.

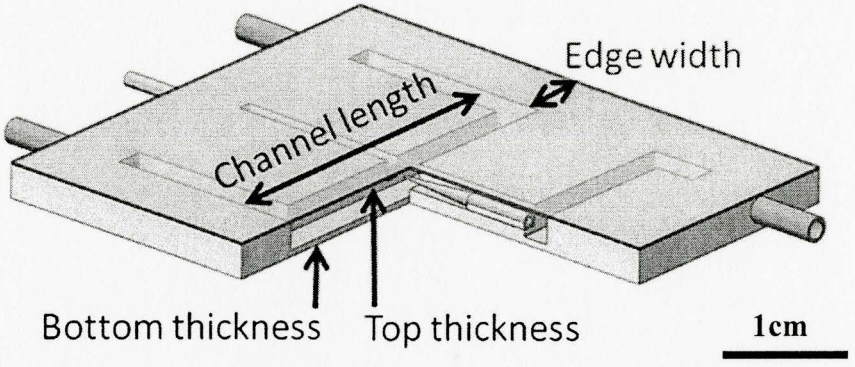

Figure 40: Parameters that were varied for simulation

Edge Width

The first parameter that was varied was the width of the material from the edge of the device to the side of the compliant channel. The width on the actual device was controlled by measuring and cutting the excess material using a scalpel and a straight edge. The width of the edge in our prototype device was 5mm. For the simulations, this width was varied from 5mm to 1mm to determine what effect this would have on the amount of displacement transferred to the needle. The results are shown in Figure 41.

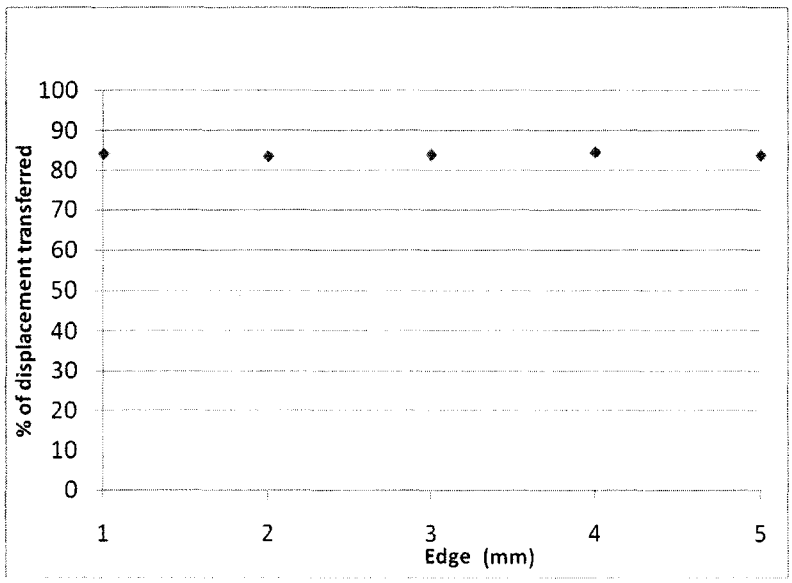

Figure 41: Edge width effect on displacement transferred

It is seen that the changes are insignificant. Reducing the width from 5mm to 1mm had the effect of changing the percentage transferred from 83.77% to 84.19%. Therefore, an increase or decrease in the edge width of the material has an insignificant effect on the amount of the applied displacement that is transferred to the needle.

Channel Length

To determine the effect of the channel length, it was varied from 25mm to 45mm. The original length for the device was 25mm. The results are shown in Figure 42.

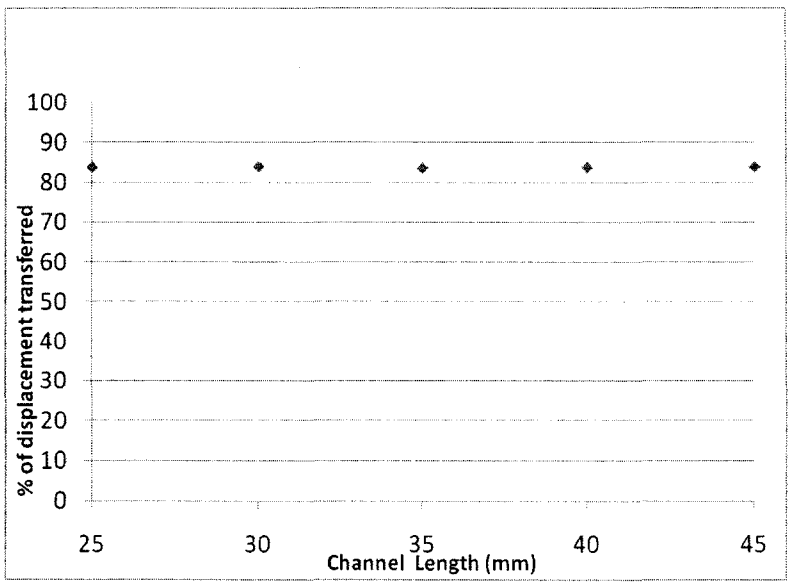

Figure 42: Variation in the channel length

It can be seen that here too the variations had only small effects on the percentage displacement transferred to the needle. Increasing the length from 25mm to 45mm changed the amount transferred from 83.77% to 83.93%. From these results it was concluded that the channel length also only plays an insignificant role in the amount of the applied displacement that is transferred for the actuation of the needle.

Channel Bottom Thickness

The bottom channel thickness was also varied to determine what effect this would have, as shown in Figure 43. The bottom thickness for both prototype devices was 0.5mm and this was varied down to 0.1mm for the simulations. From this it was found that varying the thickness of the bottom membrane had significant effects on the percentage of the applied displacement that was transferred to the needle.

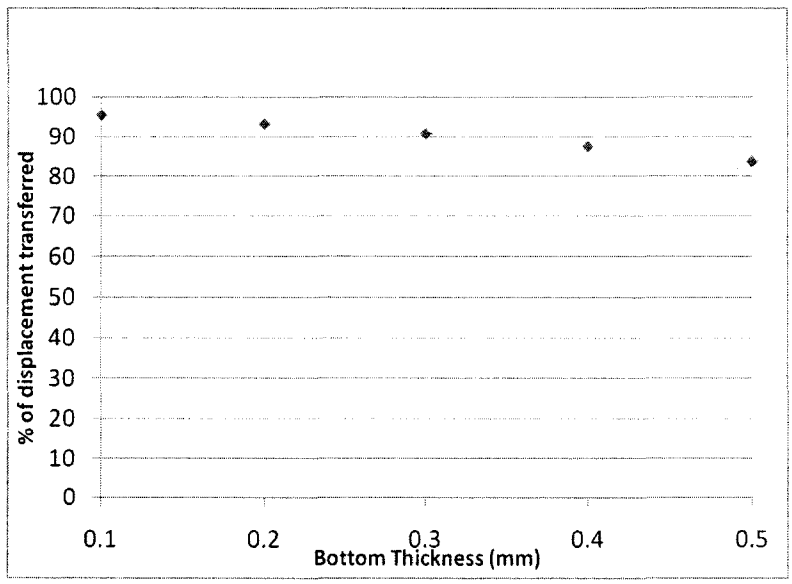

Figure 43: Channel bottom thickness variation

There was a significant change in the percentage transferred. It increased from 83.77% at 0.5mm thickness to around 92% at 0.25mm and to 95.45% at 0.1mm. Therefore, it was determined that the bottom thickness is an important geometric parameter for the device.

Channel Top Thickness

The channel top thickness was varied to determine the effect on the displacement. The original thickness for the device was 150μm and was reduced down to 50μm for the simulations. The results are shown in Figure 44.

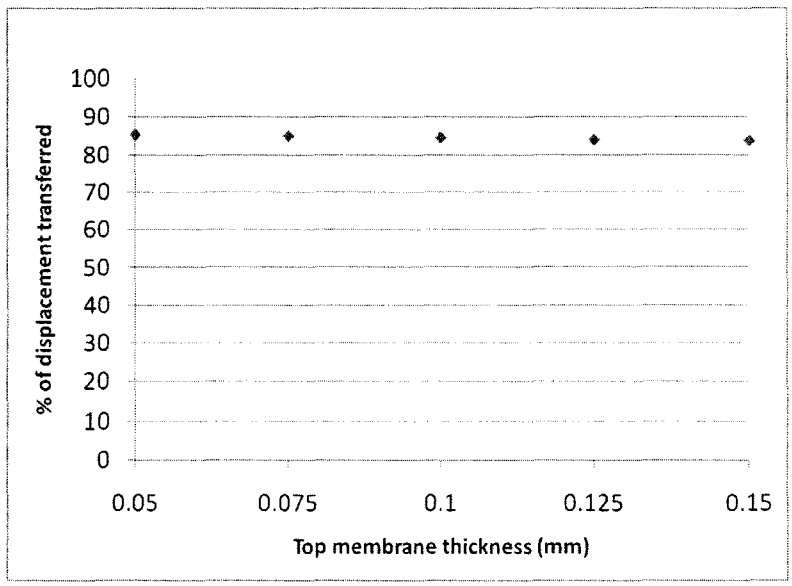

Figure 44: Top thickness variation

The simulations showed that the thickness variation had also a negligible effect on the displacement. It changed the displacement from 83.77% to 85.25%, which is small compared to the effect of other parameters. Optimizing the membrane thickness is not worth the effort to fabricate and bond membranes thinner than 150um.

Conclusion

From these simulations, it was found that the thickness of the channel bottom had the greatest impact on the amount of the applied displacement that is transferred to the needle. Therefore, this parameter needs to be carefully controlled. Control over the thickness of the bottom membrane can be achieved by spinning or casting a predetermined volume of PDMS. This will ensure repeatability between devices.

5.3.2 Electroosmotic Reagent Transport

To achieve electroosmotic flow in our device, a potential difference was applied to electrodes embedded into the target and reagent supply channels. Stainless steel needles inserted into the channels through the PDMS were used as electrodes. The potentials were applied using a Keithley 2410 power supply. The setup for the Electroosmotic pumping is shown in Figure 45.

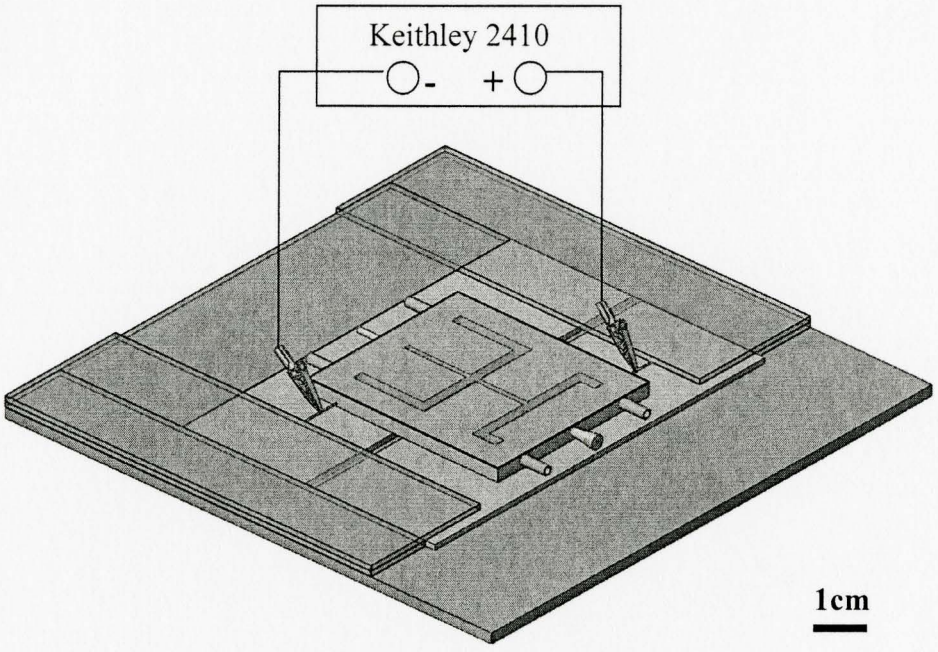

Figure 45: Electroosmotic pumping setup

Full electrical characterizations were performed for prototypes 2, 3 and 5. Firstly, the current and voltage relationship for the devices was characterized to determine the current generated as a result of the application of the potential. Initial characterizations on prototypes 2 and 3 were done using single-cell Xenopus Laevis eggs (~1mm diameter), and testing in prototype 5 was done with Zebrafish embryos (~1mm diameter).

Prototypes 2 and 3

For each device, two sets of tests were performed, one with the needle inserted into the eggs or embryos and one with the device in neutral state. For prototypes 2 and 3, the working fluids used were deionized water in the target channel and red food coloring in reagent channel. For these devices potentials between 0 and 100V were applied and the current was noted from the Keithley 2410 power supply. These results for both prototypes are shown in Figure 46.

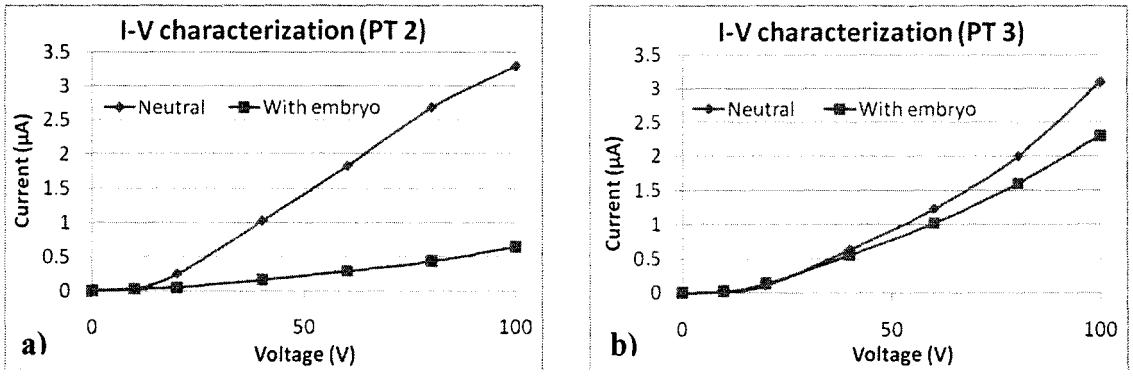

Figure 46: Current-Voltage Graphs of Prototype 2 and 3 for Xenopus Laevis egg

From these results it can be seen that the current values for the device in neutral state were approximately the same, even though the injection needle tip size (30μm and 20μm) and the length of the needles were different (16mm and 11mm). This is expected as they have the same working fluids which determine the resistance path of the electric potential. However, upon injection into the embryo the current values are different. This can be attributed to the difference in the location of the injection into the egg and due to the different amount of intra-cellular material being drawn into the injection needle upon insertion due to the difference in the needle tip sizes.

The flow rates for prototypes 2 and 3 were characterized by tracking the movement of the interface between the deionized water and the food coloring solution. The solutions were loaded into the device, and a potential was applied to completely fill the injection needle with the reagent solution, and the target channel solution was flushed. A reverse potential was then applied to cause the reverse flow of the deionized water and the food coloring solution into the injection needle. This is show in Figure 47.

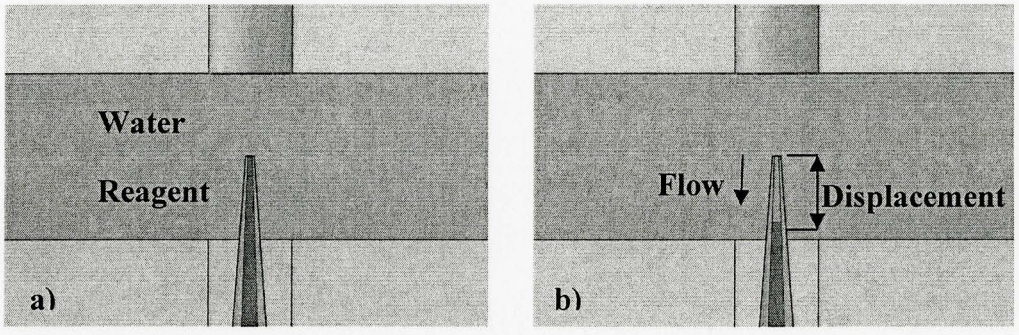

Figure 47: Measuring of electroosmotic flow rate using interface tracking

The rate at which the interface receded in the injection needle was measured by capturing videos and measuring the precise time and displacement using Adobe Premiere. The frames captured from the video allowed for the measurement of the velocity of the interface. This is shown in Figure 48 and Figure 48.

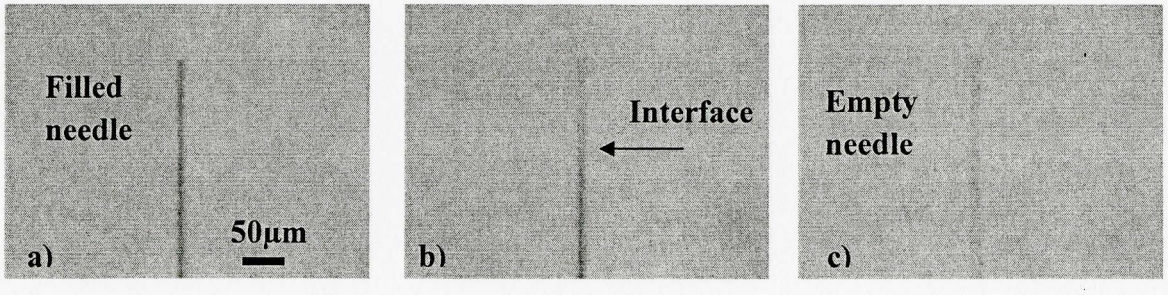

Figure 48: Flow reversal for electroosmosis measurement a.) t=0s b.) t=1.5s c.) t=3s

The flow rate was determined by measuring the needle dimensions and calculating the volume of the displaced liquid and dividing it by time passed. The following Equation 4 was used to calculate the volume of the frustum:

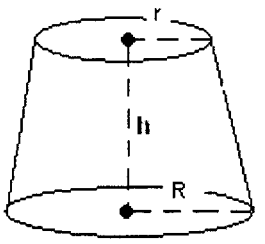

$$\text{Volume} = \frac{\pi}{3} h(R^2 + r^2 + R * r)$$

Equation 4: Formula for calculation of volume of a frustum

The flow rates obtained for prototypes 2 and 3 are shown in Figure 49. The difference in the flow rates for the two devices can be attributed to the differences in the size and the shape of the needle tips.

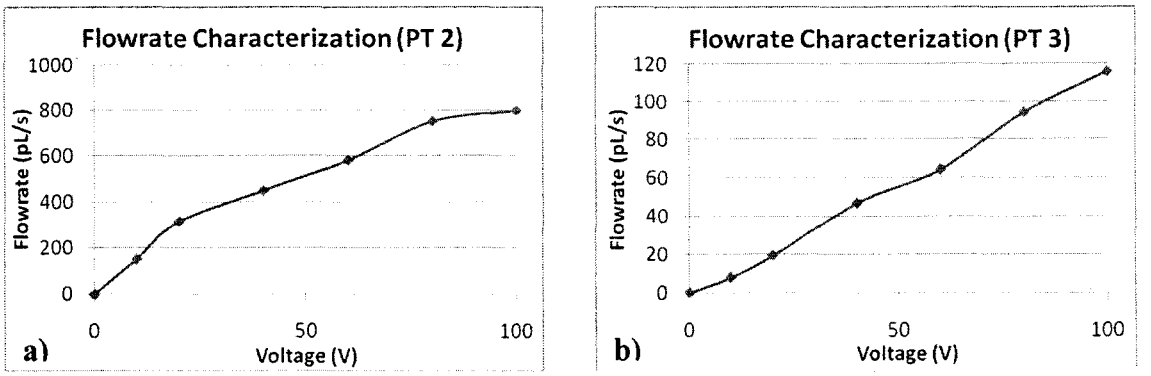

Figure 49: Flow rate Characterization Prototype 2 and 3 for Xenopus Laevis egg

The flow rate for prototype 2 at 100V was found to be 798pL/s and for prototype 3 it was 115pL/s. The currents measured at these voltages were approximately the same at 3.3μA and 3.1μA, respectively. Therefore, the difference in the flow rates for these two devices is primarily due to the geometric differences between the injection needles. The difference in the length, taper and the tip size of the injection needle (30 μm, 20μm) leads to a 7 fold decrease in the electroosmotic flow. Therefore, depending on the application, and how much reagent volume needs to be delivered, an appropriately sized injection needle needs to be chosen. This is to ensure that an adequate volume of reagent can be delivered with a very short electrical pulse to reduce exposure of the egg to the electric field and thus reduce electrical damage. However, the needle needs to be small enough to avoid damage due to the mechanical puncture. Therefore, the injection needle needs to be large enough to ensure adequate reagent delivery in short time and small enough to reduce mechanical damage to the cell.

Prototype 5

Testing for prototype 5 was performed using Zebrafish embryos instead of Xenopus Laevis, as these are transparent and therefore enable better visualization of the injections. To ensure realistic testing conditions, the combinations of solutions used for injection were those that would typically be used in Zebrafish embryo injections. The target channel contained using a solution of E3 embryo medium (consists of 5 mM NaCl, 0.17 mM KCl, 0.33 mM CaCl2·2H2O, 0.33 mM MgSO4) and reagent channel contained a solution of 1g methylene blue dissolved in 25ml ultrapure water. The results current-voltage relationship for the injection of the Zebrafish embryos using this combination of solutions is shown in Figure 50a.). The current obtained in this case is slightly higher than in prototypes 2 and 3, likely due to the difference in the working fluids.

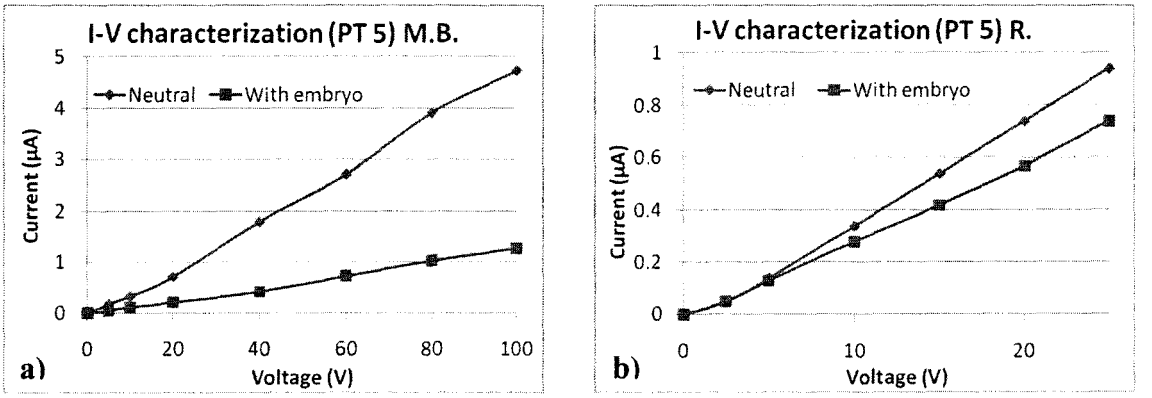

Figure 50: Current-Voltage Graphs of Prototype 5 for Zebrafish embryo

The combination of methylene blue in ultrapure water and E3 buffer medium was used in this device to ensure realistic testing conditions for actual injection experiments. However, as methylene blue has a net positive electric charge, additional experiments were required to verify that the motion of the solution in the needle was in fact due to the bulk movement (electro-osmosis) of the solution rather than ion migration (electrophoresis) due to the presence of the electric field. To verify electroosmosis, additional testing was performed using a solution of 0.2g Rhodamine in 40ml of pH 10 carbonate buffer in the reagent supply channel and pH 10 carbonate buffer in the target supply channel. This combination of Rhodamine and pH10 buffer was used as it is a neutral molecule in the pH range between 6 and 10.8 [Schrumm 2000]. This aforementioned technique is called "neutral marker method". Therefore, when there is observable flow it is entirely due to electroosmosis and not electrophoresis of the molecules. This allows for the verification and precise measurement of the electroosmotic flow. Having flow primarily due to electroosmosis is advantageous as it provides better control over the delivery volume than electrophoresis. The results obtained with the neutral marker method are shown in Figure 50b.). The voltage range used ranged from 0V-25V, as these present the most realistic injection parameters. The results obtained are highly linear and corroborate well with theory. The data follows a

predictable linear trend, with a slight curvature at the beginning of the data, which is likely caused by an over-potential. The current values for the device in neutral state reached a maximum of 0.94uA and 0.74uA with the insertion of the injection needle into the Zebrafish embryo. Based on the difference between the current values for the device in neutral state and engaged state, the resistance due to the presence of the embryo was calculated to be 7.7Mohms, which is due to intracellular materials and clogging of the needle during injection.

The flow rates for the electroosmotic flow for both combinations (methylene blue/ultrapure water and E3, and Rhodamine/deionized water, deionized water) in both prototype 5 devices were characterized. The procedure was the same as for prototypes 2 and 3. In the first instance, the flow was characterized for 0-100V, and for the second case it was done for 0-25V. The needle tip size in the first device was 10μm and in the second device it as 12μm. Here there is 3.25 fold difference in the flow rates at 25V (2.8pL/s vs. 9.1pL/s), which is primarily due to the geometric differences and the difference in the electroosmotic mobility of the reagents, since the current values obtained for the two prototype 5 devices are also approximately the same at 25V. The flow rates obtained are shown in Figure 51.

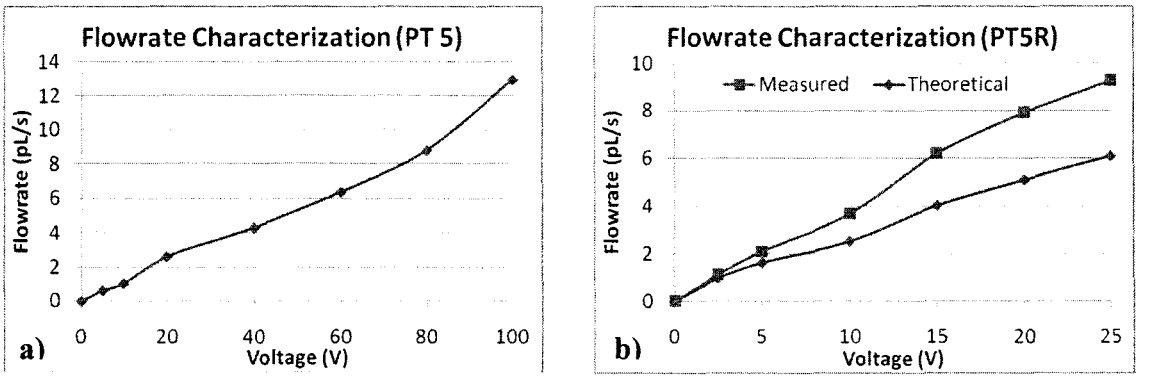

Figure 51: Flow rate vs. Voltage for Prototype 5 Injection Device

The flow rates with the needle inserted into the embryo, as shown in Figure 51 b.) were calculated theoretically due to the difficulty in measuring the actual flow rate. The methodology used to determine the flow rate was as follows. Firstly, the electroosmotic mobility of the electroosmotic flow in the injection capillary was calculated using the flow rates measured from the device in its neutral state. This was done using Equation 5:

$$\frac{Q_{eo}/A}{E_z} = \mu_{eo}$$

Equation 5: Calculation of electroosmotic mobility

where Q_{eo} is the measured electroosmotic flow rate, A is the area of the opening of the injection needle, E_z is the electrical field strength and μ_{eo} is the electroosmotic mobility. The electric field strength was calculated by dividing the potential applied to the device by the total length of the injection needle. Based on these calculates, the average electroosmotic mobility of the flow was calculated to be 4.186e-7 $m^2V^{-1}s^{-1}$. The next step was to determine the changes in the electric field due to the presence of the embryo. This was done by calculating the drop in potential caused by the added resistance due to the presence of the Zebrafish embryo. This reduced potential was then used to calculate the new electric field across the injection needle. With the electroosmotic mobility of the system and the new electric field distribution, the electroosmotic flow rates were then calculated.

The calculated theoretical flowrates due to the added resistance of 7.7Mohms of the Zebrafish embryo resulted in a 25% decrease in the flow rate. The calculated flow rates for when the needle is inserted into the Zebrafish embryo are about 6.1pL/s at 25V. The volumes used for injection of Zebrafish typically are in the 100-500 pL range, therefore it may be necessary to use slightly larger injection needles to increase flowrates to reduce the time of exposure to the electric field. If proven experimentally, this method

of calculating the flow rate during the insertion into the embryo can be used to achieve extremely precise control over the volumes delivered even when the current values during injection differ due to the different injection locations.

To determine the effects of the needle size on the flow rate, another device was fabricated with a needle tip diameter of 15μm to compare with the previous device with 12μm tip diameter. The characterization of the flowrates for this device was also conducted using rhodamine in pH 10 buffer. The results for the flowrate are shown below in Figure 52.

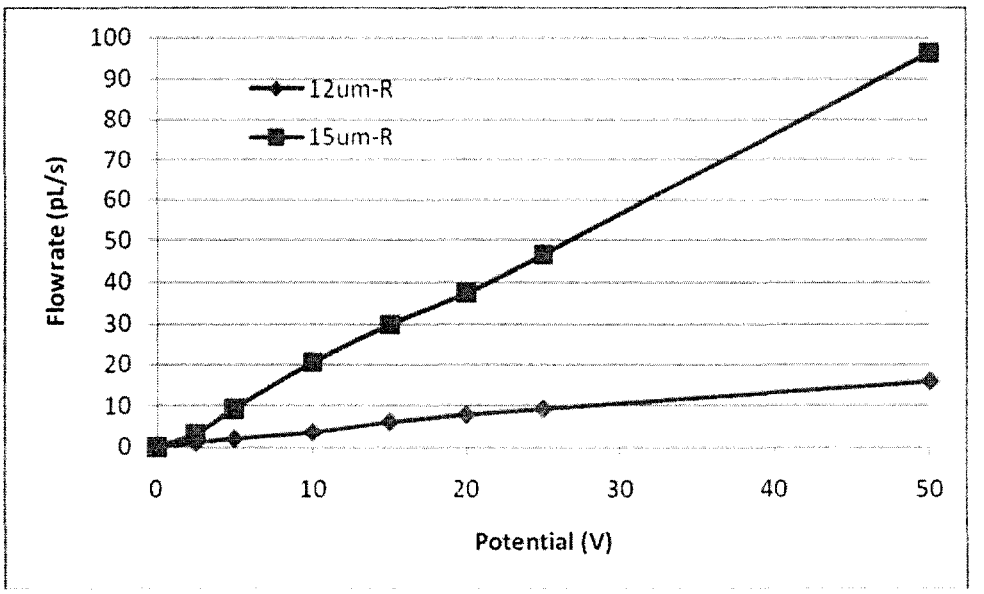

Figure 52: Comparison in flowrate between 12μm and 15μm tip.

From this it can be seen that there is an approximately 4 fold difference in the flowrates as a result of the tip diameter being larger. To determine the cause of this, the current-voltage characteristics were also compared as seen in Figure 53.

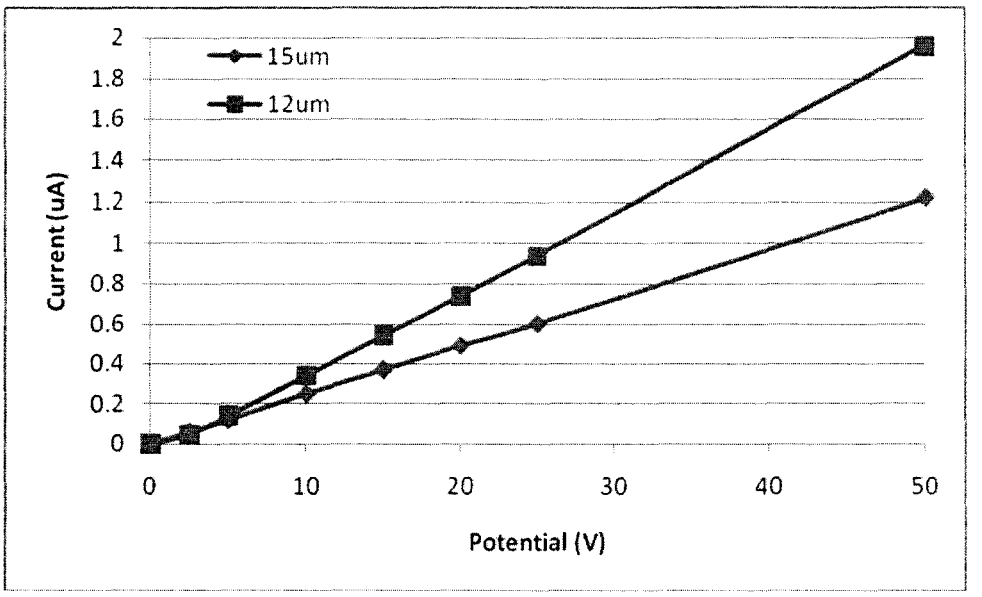

Figure 53: Current-Voltage comparison for 12um and 15um needle tip

Here it is seen that there is a 1.5 fold difference in the current between the two devices. From the previous comparison of PT2 and PT3, the electrical properties of the device for the same combination of compounds should not vary that much. Therefore, it is believed that the results for the characterization of the 12um device are skewed, possibly due to clogging of the needle by foreign particles. This may also explain the large difference in the flowrates between the two devices. Theoretically, it should vary only by a factor proportional to the difference in the injection needle tip size. Therefore, this is something that needs to be investigated by performing the characterization using new devices to obtain proper data.

5.4 Results

As aforementioned, device testing and characterization was conducted using Xenopus Laevis eggs and Zebrafish embryos. Prototypes 2 and 3 were used to inject Xenopus Laevis embryos with red food coloring. The results obtained for these prototypes are shown in Figure 54.

Figure 54: (a) Cell captured by vacuum in target supply channel. (b) Insertion of the needle into the cell by the actuation of the moving substrate. Needle is inserted and slightly retracted to prevent clogging. (c) Pumping of dye into cell by electro-osmotic flow by application of 100 V for 60s.

The prototype 5 devices were successfully used for the injection of Zebrafish embryos. The embryos were loaded into the device, immobilized by the application of suction using a syringe and subsequently injected by the needle. The results obtained for the methylene blue injection is shown in Figure 55. The injection and pumping process from the initial point of immobilization, takes approximately 15-20 seconds as the actuation of the needle is presently done manually using a micropositioner. However, if this is automated this process can be significantly improved.

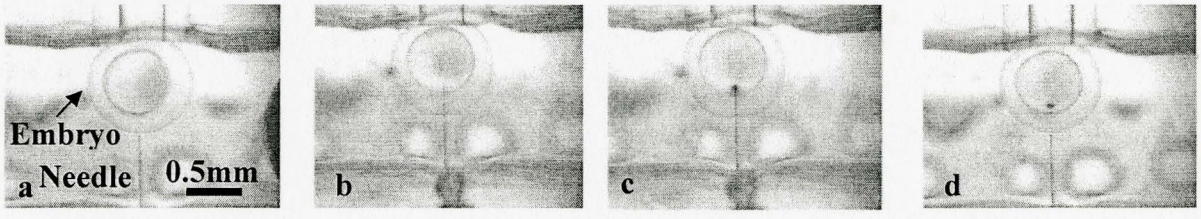

Figure 55: (a) Captured embryo (b) Insertion of needle (c) EOF injection (25V, 10s) (d) Needle withdrawal

The results for the injections of Rhodamine into the Zebrafish embryo are shown in Figure 56. The reagent was also pumped into the embryo by the applying 25V for 10s.

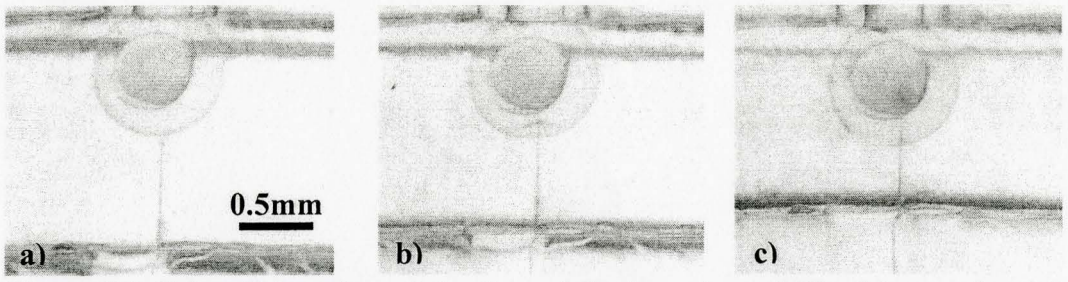

Figure 56: Zebrafish embryo injection a.) Embryo immobilized by suction b.) Needle penetrating chorion c.) Rhodamine injected into yolk sack

The injection experiments were conducted on viable embryos; however their survival rates were not assessed. It is expected that viable embryos will be obtained by tweaking the electrokinetic parameters appropriately. Possibilities include pulsing the applied potential either using AC or DC potentials. Parameters that can be adjusted are the magnitude of the pulse and the length of the applied pulse.

5.5 Summary

This chapter presented the experimental setup, characterization and results obtained from the injection device. The chapter began with the setup used for the device, and the characterization of the compliant channels of the device. From the results and the simulations for the compliant channel it was found that the most critical parameter for the optimization of the device is the thickness of the bottom membrane of the compliant channel. This thickness had the greatest effect in the percentage of the applied transfer is transferred to the needle. It is important to control this parameter as it will provide precise control over the motion of the needle with high repeatability. The chapter then highlighted the characterization of the electroosmotic injection. The results obtained followed a linear trend and correspond well to theory. Finally, the results obtained in the injection of Xenopus Laevis eggs and Zebrafish embryos were presented.

CHAPTER 6
CONTRIBUTIONS AND FUTURE WORK

6.1 Contributions

This thesis made three primary contributions to microfluidics and 'lab on a chip' technology. The system architecture enables high-throughput injections which can be integrated with pre and post processing operations. Secondly, the use of compliant fluidic channels for the actuation of components in PDMS is novel. And finally, it introduces the use of electroosmotic flow for injection for precise electric dosage control.

6.1.1 Injections in a 'Lab on a Chip' format

The research that was conducted as part of this Masters degree has resulted in the design and fabrication of a novel 'Lab on a Chip' device that has enabled capillary injections to be performed in an integrated fluidic format. The device maintains the positive aspects of capillary microinjection such as low cytotoxicity, quantitative and targeted delivery (cytoplasm or nucleus) without cell or reagent restrictions, while eliminating the negative aspects such as low-throughput and injection variability due to varying operator skill. The system architecture is fully scalable and can be further miniaturized for smaller cells. Additionally, it enables multiple parallel injections as well

as automation. Another advantage is that it allows for the complete integration of pre and post processing operations such as sorting and analysis in a high-throughput fashion. These features will enable the use of microinjection for large clinical applications which was previously not possible.

6.1.2 Compliant Fluidic Channels

In our device the actuation of the integrated needle is achieved by the compliant deformation of the flexible PDMS structure. Although the flexible nature of PDMS has been used for components such as pumps and valves, it had never been applied to fluidic channels. The actuation of embedded components within PDMS by the application of an external deformation is also entirely novel. What is also novel is the arrangement of the suction capillary and injection needle. Injections occur in a planar configuration which provides precise control over the injection location. Only a single degree of freedom is required for operation, thus greatly simplifying injections and eliminating damage due to lateral motion.

6.1.3 Electroosmotic Dosage Control

In our device we displayed reagent delivery by electroosmotic flow, rather than pressure driven flow. This enabled us to overcome limitations of traditional microinjection such as the needle tip size and minimum reagent volume. The use of electroosmosis for reagent injection provides a number of advantages over pressure driven flow such as the absence of moving parts, precise electrical control over flow and virtually unlimited resolution. This will enable true miniaturization of the device as it does not rely on external pumps. Furthermore, since electroosmotic flow exhibits plug flow it provides better dosage control than pressure driven flow. The application of electroosmosis for single cell or embryo injections is entirely novel, and if proven viable can significantly improve dosing and repeatability of injection experiments.

6.2 Future Work

The immediate future work pertaining to this project would be to perform viability studies with using electroosmotic flow for injections. Parameters such as the type of potential (AC vs. DC), the potential levels and the application method of the potential (pulsing or continuous) would have to be optimized to determine the parameters that yield viable injections.

There are a number of aspects of the device that can be improved and enhanced. Firstly, the injections are presently performed manually using a microactuator. This could be automated using a precision motor to drive the movable substrate to enable more rapid injections. Furthermore, an optical control system could be developed to detect the presence of an embryo within the channel, and automatically engage the suction channel to immobilize the embryo. The insertion of the needle into the embryo could then proceed in an automated fashion.

Another component of the device that can be improved is the repeatability between different devices. The performance presently varies as the injection needles that are used are fabricated using a micropipette puller and therefore the needle dimensions vary. As a result of this, the flow and injection characteristics of individual devices also vary. By using uniform injection needles, such as etched fused silica capillaries with identical tip diameters and constant inner diameters, injection repeatability across different devices could be significantly improved.

In order to enable the widespread adoption of the device, another issue that needs to be addressed is the replacement of contaminated and broken or clogged needles. Therefore, a method has to be devised that will allow for the injection needle to be replaced in the device without having to fabricate an entirely new device. This will make the device more practical and will increase the possibility that it will be adopted and used in labs that do not have access to microfabrication facilities.

Finally, once these aspects of the embryo injection device are addressed, the entire device could be further miniaturized to enable the injection of small cells with diameters in the 10s of microns.

BIBLIOGRAPHY

[Adamo 2008] Adamo, A. and K. F. Jensen (2008). "Microfluidic based single cell microinjection." Lab on a Chip **8**: 1258-1261.

[Andersson 2004] Andersson, H. and A. van den Berg (2004). "Microtechnologies and nanotechnologies for single-cell analysis." Current Opinion in Biotechnology **15**(1): 44-49.

[Bassous 1977] Bassous, E., H. H. Taub, et al. (1977). "Ink jet printing nozzle arrays etched in silicon." Applied Physics Letters **31**: 135.

[Chun 1999] Chun, K., G. Hashiguchi, et al. (1999). "Fabrication of Array of Hollow Microcapillaries Used for Injection of Genetic Materials into Animal/Plant Cells." JAPANESE JOURNAL OF APPLIED PHYSICS PART 2 LETTERS **38**: 279-281.

[Beebe 2002] David, J. B., A. M. Glennys, et al. (2002). "Physics and Applications of Microfluidic in biology." Annu. Rev. Bimed. Eng. v4, pp261-86.

[Devasenathipathy 2003] Devasenathipathy, S. and J. G. Santiago (2003). Electrokinetic Flow Diagnostics" in Breuer, KS, Ed., Micro-and Nano-Scale Diagnostic Techniques, Springer Verlag, New York.

[Dittrich 2006] Dittrich, P. S. and A. Manz (2006). "Lab-on-a-chip: microfluidics in drug discovery." Nature Reviews Drug Discovery **5**(3): 210.

[Fox 2006] Fox, M. B., D. C. Esveld, et al. (2006). "Electroporation of cells in microfluidic devices: a review." Analytical and Bioanalytical Chemistry **385**(3): 474-485.

[Fukui 1996] Fukui, Y., E. S. Lee, et al. (1996). Effect of medium renewal during culture in two different culture systems on development to blastocysts from in vitro produced early bovine embryos, Am Soc Animal Sci. **74:** 2752-2758.

[Le Gac 2007] Gac, S. L., E. Zwaan, et al. (2007). "Sonoporation of suspension cells with a single cavitation bubble in a microfluidic confinement." Lab on a Chip **7**(12): 1666-1672.

[Gehl 2003] Gehl, J. (2003). "Electroporation: theory and methods, perspectives for drug delivery, gene therapy and research." Acta Physiologica Scandinavica **177**(4): 437-447.

[Hsu 2004] Hsu, C. H., C. Chen, et al. (2004). ""Microcanals" for micropipette access to single cells in microfluidic environments." Lab on a Chip **4**(5): 420-424.

[Huang 2003] Huang, Y. and B. Rubinsky (2003). "Flow-through micro-electroporation chip for high efficiency single-cell genetic manipulation." Sensors & Actuators: A. Physical **104**(3): 205-212.

[Ionescu-Zanetti 2008] Ionescu-Zanetti, C., A. Blatz, et al. (2008). "Electrophoresis-assisted single-cell electroporation for efficient intracellular delivery." Biomedical Microdevices **10**(1): 113-116.

[Jähne 1955] Jähne, A., D. Becker, et al. (1955). "Genetic engineering of cereal crop plants: a review." Euphytica **85**(1): 35-44.

[Jensen 2001] Jensen, K. F. (2001). "Microreaction engineering—is small better?" Chemical Engineering Science **56**(2): 293-303.

[Kallio 2006] Kallio, P. and J. Kuncová-Kallio (2006). "Capillary pressure microinjection of living adherent cells: Challenges in automation." Journal of Micromechatronics **3**(3): 189-220.

[Khine 2007] Khine, M., C. Ionescu-Zanetti, et al. (2007). "Single-cell electroporation arrays with real-time monitoring and feedback control." Lab on a Chip **7**(4): 457-462.

[Kurosawa 2006] Kurosawa, O., H. Oana, et al. (2006). "Electroporation through a micro-fabricated orifice and its application to the measurement of cell response to external stimuli." Measurement Science and Technology **17**(12): 3127-3133.

[Lee 2003] Lee, S., W. Jeong, et al. (2003). "Microfluidic valve with cored glass microneedle for microinjection." Lab on a Chip **3**(3): 164-167.

[Lin 2001] Lin, Y. C., C. M. Jen, et al. (2001). "Electroporation microchips for continuous gene transfection." Sensors & Actuators: B. Chemical **79**(2-3): 137-143.

[Lin 2003] Lin, Y. C., M. Li, et al. (2003). "A microchip for electroporation of primary endothelial cells." Sensors & Actuators: A. Physical **108**(1-3): 12-19.

[Liu 2006] Liu, Y., H. Yang, et al. (2006). "Ultrasound: Mechanical gene transfer into plant cells by sonoporation." Biotechnology Advances **24**(1): 1-16.

[Lo 1983] Lo, C. W. (1983). "Transformation by iontophoretic microinjection of DNA: multiple integrations without tandem insertions." Molecular and Cellular Biology **3**(10): 1803-1814.

[Lukkari 2004] Lukkari, M. J., M. I. Karjalainen, et al. (2004). Electrical detection of the contact between a microinjection pipette and cells.

[Luo 2000] Luo, D. and W. M. Saltzman (2000). "Synthetic DNA delivery systems." Nature Biotechnology **18**: 33-37.

[Matsuoka 2005] Matsuoka, H., T. Komazaki, et al. (2005). "High throughput easy microinjection with a single-cell manipulation supporting robot." Journal of Biotechnology **116**(2): 185-194.

[McDonald 2002] McDonald, J. C. and G. M. Whitesides (2002). "Poly (dimethylsiloxane) as a Material for Fabricating Microfluidic Devices." ACCOUNTS OF CHEMICAL RESEARCH **35**(7): 491-500.

[Mehier-Humbert 2005] Mehier-Humbert, S., T. Bettinger, et al. (2005). "Ultrasound-mediated gene delivery: Kinetics of plasmid internalization and gene expression." Journal of Controlled Release **104**(1): 203-211.

[Mehier-Humbert 2004] Mehier-Humbert, S. and R. H. Guy (2004). "Physical methods for gene transfer: Improving the kinetics of gene delivery into cells." Advanced Drug Delivery Reviews **57**(5): 733-753.

[Miller 2002] Miller, D. L., S. V. Pislaru, et al. (2002). "Sonoporation: Mechanical DNA Delivery by Ultrasonic Cavitation." Somatic Cell and Molecular Genetics **27**(1): 115-134.

[Minaschek 1989] Minaschek, G., J. Bereiter-Hahn, et al. (1989). "Quantitation of the volume of liquid injected into cells by means of pressure." Exp Cell Res **183**(2): 434-42.

[Mitchell 2001] Mitchell, P. (2001). "Microfluidics—downsizing large-scale biology." Nature Biotechnology **19**: 717-721.

[Nguyen 2006] Nguyen, N. and S. H. Chan (2006). "Micromachined polymer electrolyte membrane and direct methanol fuel cells-a review." JOURNAL OF MICROMECHANICS AND MICROENGINEERING **16**(4): 1.

[Noori 2008] Noori, A., Selvaganapathy, P.R., Upadhyaya, S. (2008). Materials and Microfabrication Processes for Microfluidic Devices, in "Microfluidics for Biological Applications", Finehout, E., Tian, W.C. (Eds.). Springer Science & Business Media, LLC.

[Noori 2008-1] Noori, A., Selvaganapathy, P.R. (2008), "Single Cell Microinjection using Compliant Fluidic Channels", Proceedings of 12th Internat. Conference on Miniaturized Systems for Chemistry and Life Sciences (MicroTAS 2008.

[Ny 2006] Ny, A., M. Autiero, et al. (2006). "Zebrafish and Xenopus tadpoles: Small animal models to study angiogenesis and lymphangiogenesis." Experimental Cell Research **312**(5): 684-693.

[Paegel 2003] Paegel, B. M., R. G. Blazej, et al. (2003). "Microfluidic devices for DNA sequencing: sample preparation and electrophoretic analysis." Current Opinion in Biotechnology **14**(1): 42-50.

[Paik 2008] Paik, P. Y., V. K. Pamula, et al. (2008). "A Digital-Microfluidic Approach to Chip Cooling." IEEE Design and Test of Computers **25**(4): 372.

[Parker 2004] Parker, A. L., C. Newman, et al. (2004). "Nonviral gene delivery: techniques and implications for molecular medicine." Expert Reviews in Molecular Medicine **5**(22): 1-15.

[Parker 1997] Parker, S. P. (1997). McGraw-Hill dictionary of chemistry, McGraw-Hill New York.

[Pilarski 2004] Pilarski, L. M., S. Adamia, et al. (2004). Improved diagnosis and monitoring of cancer using portable microfluidics platforms.

[Potter 1988] Potter, H. (1988). "Electroporation in biology: Methods, applications, and instrumentation." Analytical Biochemistry **174**(2): 361-373.

[Pugia 2005] Pugia, M. J., G. Blankenstein, et al. (2005). Microfluidic Tool Box as Technology Platform for Hand-Held Diagnostics, Am Assoc Clin Chem. **51:** 1923-1932.

[Purves 1980] Purves, R. (1980). "Ionophoresis - Progress and Pitfalls." TINS **3**: 245-247.

[Purves 1979] Purves, R. D. (1979). "The physics of iontophoretic pipettes." J Neurosci Methods **1**(2): 165-78.

[Rice 1965] Rice, C. L., R. Whitehead, "Electrokinetic flow in a narrow cylindrical capillary", J. Phys. Chem. Vol.69, pp.4017- 4029, 1965.

[Schrum 2000] Schrum, K. F., J. M. Lancaster, et al. (2000). "Monitoring Electroosmotic Flow by Periodic Photobleaching of a Dilute, Neutral Fluorophore." ANALYTICAL CHEMISTRY-WASHINGTON DC- **72**(18): 4317-4321.

[Sedgwick 2008] Sedgwick, H., F. Caron, et al. (2008). "Lab-on-a-chip technologies for proteomic analysis from isolated cells." Journal of The Royal Society Interface **5**: 123-130.

[Sia 2004] Sia, S. K., V. Linder, et al. (2004). "An integrated approach to a portable and low-cost immunoassay for resource-poor settings." Angewandte Chemie(International ed. Print) **43**(4): 498-502.

[Squires 2005] Squires, T. M. and S. R. Quake (2005). "Microfluidics: Fluid physics at the nanoliter scale." Reviews of Modern Physics **77**(3): 977-1026.

[Storms 1998] Storms, M. M. H., C. va, et al. (1998). "A comparison of two methods of microinjection for assessing altered plasmodesmal gating in tissues expressing viral movement proteins." The Plant Journal **13**(1): 131-140.

[Takahashi 2007] Takahashi, K., K. Tanabe, et al. (2007). "Induction of Pluripotent Stem Cells from Adult Human Fibroblasts by Defined Factors." Cell.

[Valero 2008] Valero, A., J. N. Post, et al. (2008). "Gene transfer and protein dynamics in stem cells using single cell electroporation in a microfluidic device." Lab on a Chip **8**(1): 62-67.

[Wall 1997] Wall, R. J., D. E. Kerr, et al. (1997). "Transgenic Dairy Cattle: Genetic Engineering on a Large Scale." Journal of Dairy Science **80**(9): 2213-2224.

[Walton 1987] Walton, J. R., J. D. Murray, et al. (1987). "Zygote viability in gene transfer experiments." Biology of Reproduction **37**(4): 957-967.

[Wang 2006] Wang, H. Y. and C. Lu (2006). "Electroporation of Mammalian Cells in a Microfluidic Channel with Geometric Variation." Anal. Chem **78**(14): 5158-5164.

[Wang 2007] Wang, W., F. Zhou, et al. (2007). "Measurement of electroosmotic flow in capillary and microchip electrophoresis." Journal of Chromatography A **1170**(1-2): 1-8.

[Wang 2007-1] Wang, W. H., X. Y. Liu, et al. (2007). Autonomous Zebrafish Embryo Injection Using a Microrobotic System. Proceedings of the 3rd Annual IEEE Conference on Automation Science and Engineering.

[Zhang 2006] Zhang, C., J. Xu, et al. (2006). "PCR microfluidic devices for DNA amplification." Biotechnology Advances **24**(3): 243-284.

[Zhang 2008] Yan Zhang, L.-C. Y. (2008). "Single-cell microinjection technology in cell biology." BioEssays **30**(6): 606-610.

[Zappe 2006] Zappe, S., M. Fish, et al. (2006). "Automated MEMS-based Drosophila embryo injection system for high-throughput RNAi screens." Lab on a Chip **6**(8): 1012-1019.

APPENDIX

APPENDIX A: Device Fabrication Process

1. Fabricate ABS mold using 3D polymer printer
2. Mix 1:30 PDMS, degas in vacuum desicator.
3. Place ABS mold onto levelling table and slowly pour PDMS into the mold until it reaches the top of the surrounding edges
4. Cover device and leave over night to allow PDMS to solidify, then place ABS mold with PDMS cast onto hotplate at 65C for 15 minutes
5. Peel PDMS substrate from mold and cut into appropriate size
6. Place two glass slides into device base assembly with 2mm gap between them, apply small amount of prepolymer PDMS onto PDMS substrate and bond it onto the glass slides with the walls of the channels aligned to the edges of the glass slide. Place onto hotplate at 65C for 15 minutes
7. Cleave pulled borosilicate microinjection capillary and regular 1mm OD/0.5mm ID borosilicate capillary to required size and align into the ridges perpendicular to the target channel. Use tweezers to break the tip of the injection needle off if it is too fine or if it extends too far into the channel. Adjust the needle to ensure that it protrudes approximately 1mm into the channel.
8. Deposit drops of pre-polymer PDMS into the ridges to seal the suction capillary and injection needle into place. Place onto hotplate at 95C for 10 minutes, and repeat application of PDMS if necessary to ensure proper seal.
9. Create inlet and outlet ports with 2mm OD and 1.8mm ID capillaries. Punched through the ends of the channel structures using 18 gage needle and insert cleaved capillaries. Sealed and bond into place by the deposition of pre-polymer PDMS and place onto hotplate at 95C for 10 minutes.
10. Coat silicon wafer with 1.5 μm of parylene. Fabricate 150μm PDMS membrane by spinning 1:30 volumetric ratio of PDMS for 60 seconds at 400rpm. Place

wafer with spun PDMS onto hotplate at 95C for 10 minutes. Peel and cut into appropriately sized rectangles.

11. Evenly distribute a thin layer of 1:30 volumetric ratio of liquid pre-polymer PDMS on the device and slowly roll the 150um PDMS membrane on. Prevent air bubbles from being trapped beneath the deposited membrane. Place onto hotplate at 65C for 15 minutes.

APPENDIX B: Device Automation Schematic and Post Processing

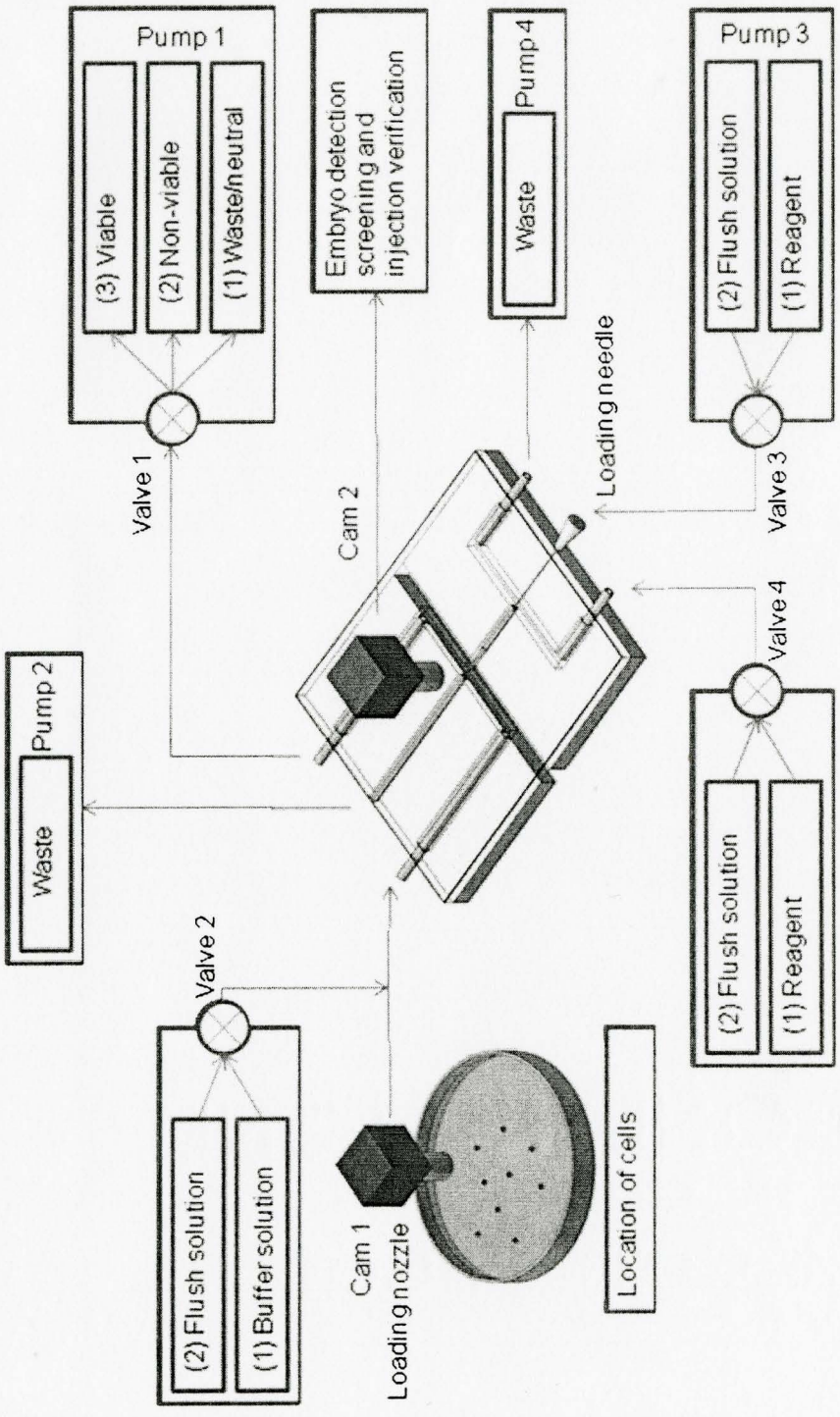

INJECTION DEVICE (PROTOTYPE 5) OPERATION PROCESS FLOW

Setup

Supply channel

1. Valve 1 set to position 1, valve 2 closed
2. Lower loading nozzle into Petri dish filled with buffer solution to load buffer solution into nozzle and embryo supply channel using suction applied to pump 1 at position 1 and stop pump 1 when channels are filled.

Reagent channel

3. Valve 4 closed, valve 3 set to position 1. Apply pump 3 to load reagent into injection needle using loading needle.
4. Valve 4 set to position 1. Apply pump 4 to load reagent into reagent channel.
5. Close valve 3 and 4.

Embryo location and loading

6. Use cam 1 to optically located embryo in Petri dish and lower loading nozzle
7. Set valve 1 to position 1 (waste/neutral reservoir) and apply suction using pump 1 to load embryo into nozzle
8. Stop suction at pump 1 and raise loading nozzle head
9. Set valve 2 to position 1 and continue to apply suction using pump 1 at valve position 1

Embryo capture and injection

10. Use cam 2 to detect embryo position as it nears suction channel then engage pump 2 and stop pump 1 once embryo has been captured.
11. Actuate needle into embryo and apply appropriate potential for electro-osmotic injection or pressure for pressure driven injection and retract needle
12. Use cam 2 to verify injection (location of needle during injection or fluorescence detection). Based on verification results set valve 1 to position 2 (non-viable) or 3 (non-viable) and apply suction to pump 1 to continue transport of embryo into reservoir

Flushing of device

Reagent channel

13. Set valve 3 to position 2, engaged pump 3 to flush solution through injection needle.
14. Set valve 4 to position 2, engage pump 4 to flush reagent channel.

Supply channel

15. Set valve 1 to position 1 and engage pump 1 to clear out loading nozzle and supply channel.
16. Engage pump 2 to clear out suction channel.
17. Set valve 2 to position 2, and valve 1 to position 1 to pump flush solution through supply channel

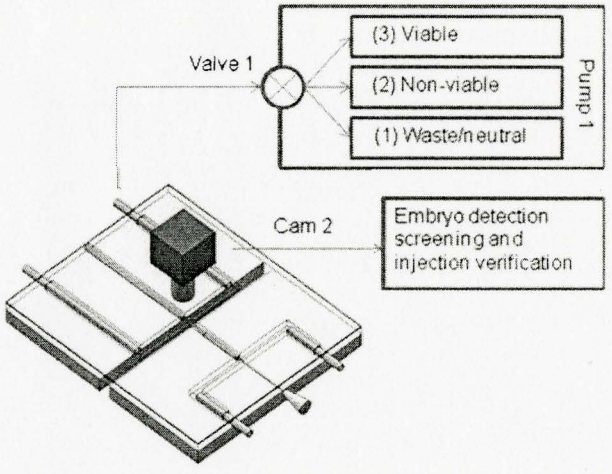

Pre-injection Screening

•Screen the captured embryos prior to injection to determine viability.
- •If viable, proceed to inject embryo.
- •If non-viable release embryo and engage pump 1 to reservoir 2.

Post-injection Screening

•Screen embryos after injection to verify viability and location of injection (e.g.: using fluorescence)
- •If viable, release embryo and engage pump 1 to reservoir 3
- •If non-viable release embryo and engage pump 1 to reservoir 2.

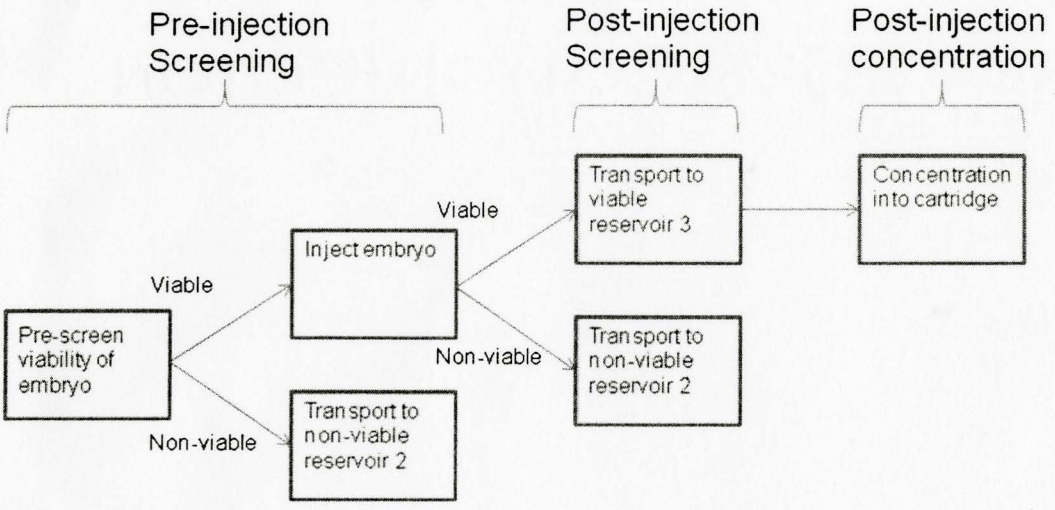

Embryo screening/sorting process flow

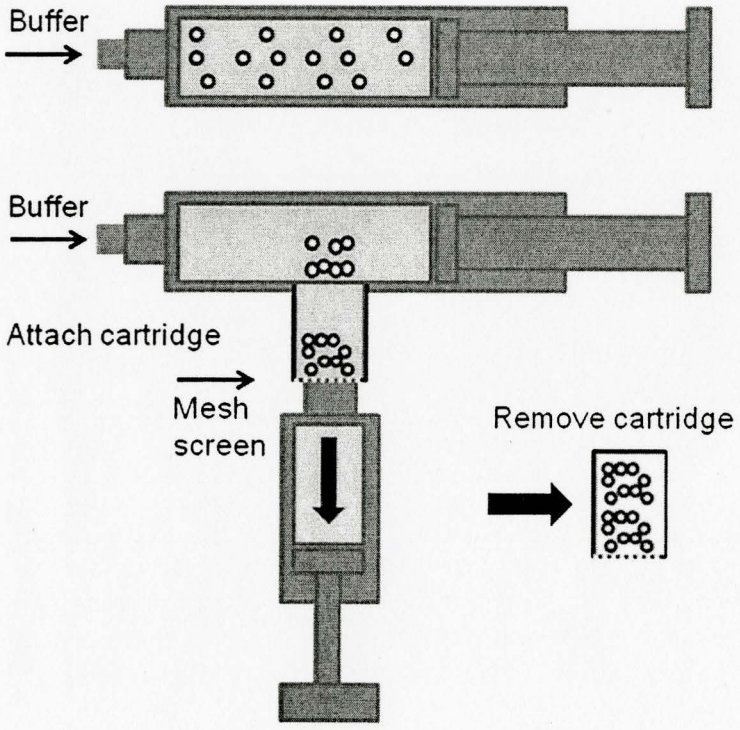

Embryo Concentration

- When injections are completed a cartridge with a mesh screen, attached to a syringe is connected to reservoir 3 and suction is applied until all embryos have been recovered from the reservoir.
- The cartridge is then removed with the embryos, and can now be transported to the breeding tank